Peptidylarginine deiminase 4 inhibition ameliorates bleomycin-induced Neutrophil extracellular traps (NETs) and fibrosis in the lungs of mice

（PAD4 阻害はマウス肺のブレオマイシン誘導 NETs と線維化を改善させる）

千葉大学大学院医学薬学府

先端医学薬学専攻

（主任：巽　浩一郎　教授）

鈴木　優毅

Title

Peptidylarginine deiminase 4 inhibition ameliorates bleomycin-induced Neutrophil extracellular traps (NETs) and fibrosis in the lungs of mice

Author

Masaki Suzuki

Affiliations

Department of Respirology, Graduate School of Medicine, Chiba University, 1-8-1, Inohana, Chuo-ku, Chiba-city, Chiba 260-8677, Japan

*Corresponding author:
Masaki Suzuki
Department of Respirology, Graduate School of Medicine, Chiba University, Chiba, Japan
1-8-1 Inohana, Chuo-ku, Chiba-shi, Chiba 260-8677, Japan
Phone: +81 43 222 7171
FAX: +81 43 226 2176
E-mail address: suzuki-m.7447@chiba-u.jp

Abstract

Idiopathic pulmonary fibrosis is a progressive fibrosing interstitial pneumonia, in which neutrophil accumulation in the lung is associated with poor prognosis. Excessive release of neutrophil extracellular traps (NETs) has been implicated in several organ fibrosis. NETs constitute a phenomenon, in which decorated nuclear chromatin with cytosolic proteins is released into the extracellular space. Peptidylarginine deiminase (PAD) 4 plays an important role in the formation of NETs. However, so far, the role of NETs in the pathogenesis of pulmonary fibrosis has been undefined. Here, we identified NETs in the alveolar and interstitial lung space of mice undergoing bleomycin (BLM) induced lung fibrosis, which was suppressed by a pan-PAD inhibitor, Cl-amidine. *In vitro*, BLM directly induced NETs in blood neutrophils, which was also inhibited by Cl-amidine. Furthermore, *Padi4* gene knockout (PAD4-KO) in mice led to the alleviation of BLM-induced NETs and pulmonary fibrosis, and expression of inflammatory and fibrotic genes. The deficiency of PAD4 prevented the decrease in the number of alveolar epithelial and pulmonary vascular endothelial cells and the increase of α-smooth muscle actin positive mesenchymal cells. Grafts of hematopoietic cells from PAD4-KO but not from wild-type (WT) mice resolved the BLM-induced lung fibrosis in WT mice, suggesting that expression of PAD4 in hematopoietic cells might be involved in the development of lung fibrosis. These data suggested that the deficiency of PAD4 could ameliorate BLM-induced formation of NETs and lung fibrosis, thus indicating that this pathway could serve as a therapeutic target for the treatment of pulmonary fibrosis.

Keywords

peptidylarginine deiminase 4,
neutrophil,
neutrophil extracellular trap,
citrullinated histone H3,
bleomycin,
pulmonary fibrosis

Introduction

Idiopathic pulmonary fibrosis (IPF) is characterized by a specific form of chronic, progressive, fibrosing interstitial pneumonia of unknown causes (1). Although the precise mechanism of the development of pulmonary fibrosis remains unclear, previous studies suggested that it might be caused by repetitive micro lung injury, chronic abnormal tissue repair and activation of fibroblasts, resulting in irreversible aberrant tissue remodeling (2). Both innate and adaptive immune mechanisms have been shown to contribute to fibrogenesis at several cellular and non-cellular levels (3, 4). A recent large cohort genome-wide association study demonstrated a link between some immune modulating genes and inflammatory processes, and therefore there has been an increased focus on the contribution of the innate immunity and inflammation to the processes of pulmonary fibrosis (3-5).

Among innate immune cells, the contribution of neutrophils to the pathogenesis of pulmonary fibrosis has been long debated. Neutrophils are the most abundant white blood cells in circulation and play a key role in innate and adaptive immunity (6). They have diverse phenotypes and are known to be associated with various pathophysiologies, such as auto-immune diseases, chronic inflammatory diseases, cancer, and tissue repair (7). Moreover, they produce neutrophil elastase (NE), matrix metalloproteases (MMPs) and tissue inhibitors of MMPs, regulating extracellular matrix components (3, 6). Particularly, NE, a neutrophil specific serine protease, has been reported to promote fibroblast proliferation and differentiation to myofibroblasts, and transforming growth factor β1 (TGFβ1) activation (8). Bronchoalveolar lavage (BAL) neutrophilia is recognized in IPF (9), and the latest international IPF guideline addressed the increase of neutrophils in BAL fluid (BALF) in support of IPF diagnosis (1). In fact, the baseline levels of BAL neutrophils predicted early mortality in patients with IPF (10). Neutrophils were also observed in the lung alveolar space nearby small alveolar damage lesions of stable cases of IPF (11). Previous reports showed elevation of key factors of chemotaxis and growth factors for neutrophils, interleukin-8 (IL-8) and chemokine ligand 18 in the lungs of patients with IPF (12). Collectively, these evidences support a pivotal role of neutrophils on the development and progression of pulmonary fibrosis. However, the precise role of neutrophils in the pathogenesis of lung fibrosis remains undefined.

Neutrophil extracellular traps (NETs), in addition to chemotaxis, phagocytosis and degradation, is one of the neutrophil functions first reported by Brinkmann V. (13). Through chromatin decondensation, activated neutrophils have been shown to release NETs in the form of web-like structures decorated with nuclear chromatin and cytosolic proteins into the extracellular space (13-16). Citrullination is the posttranslational deamination of arginine residues to citrullines, mediated by peptidylarginine deiminases (PADs), resulting in chromatin decondensation (17, 18). Histone citrullination reported to be proceeded by PADs, particularly PAD4, leads to the production of citrullinated histone H3 (citH3), which is considered a key process in the formation of NETs. While NETs exhibit antimicrobial activity, the excessive expression of NETs has been demonstrated to cause organ damage and sepsis in acute respiratory distress syndrome (ARDS) (19) and to also drive pathophysiological conditions of non-infectious diseases, such as autoimmune diseases (15, 16), deep vein thrombosis (20), transfusion-related acute lung injury (21), tumorigenesis (22), diabetes (23), and atherosclerosis (24). Regarding respiratory diseases, NETs were observed in the sputum or lungs of patients with ARDS (19), chronic obstructive pulmonary disease (25), neutrophilic asthma (25), non-specific interstitial pneumonia (NSIP) (26), and cystic fibrosis (27). Recent studies have demonstrated the close relationship between NETs and fibrosis in several organs, including the lungs. The existence of NETs in the lungs of patients with NSIP (26), and the increase of components of NETs and decrease of deoxyribonuclease I (DNAse-1), a degrader of NETs, in patients of polymyositis/dermatomyositis (PM/DM) with interstitial lung

disease (ILD) were also noted (28). In addition, fibroblasts were shown to undergo transdifferentiation to collagen-depositing myofibroblasts after incubation with NETs *in vitro*, and NETs were identified in proximity to α-smooth muscle actin (SMA)-positive fibroblasts in tissue sections from patients with fibrotic ILD (26). Another group demonstrated that limiting the activity of PAD4 and released NETs protected organs from age-related fibrosis (29).

However, the role of NETs in the pathogenesis of pulmonary fibrosis *in vivo* has been unclear to this day. In our study, we sought to examine whether NETs are induced in the lungs of mice during pulmonary fibrosing process by bleomycin (BLM) instillation. In addition, by using *Padi4* gene knockout (PAD4-KO) mice, we also sought to examine whether BLM-induced NETs and fibrosis in the lungs could be regulated by deficiency of PAD4.

Materials and Methods

Mice

Male C57BL/6 mice were purchased from Clea Japan (Tokyo, Japan). PAD4$^{-/-}$ mice on a C57BL/6 background were purchased from Jackson Laboratory (Bar Harbor, ME, USA). All animal experiments were reviewed and approved by the Review Board for animal experiments of Chiba University.

Bronchoalveolar lavage analysis

After intratracheal administration with BLM (Nippon Kayaku, Tokyo, Japan) dissolved in 100 μL saline (Otsuka Pharmaceutical Factory, Tokyo, Japan) or vehicle, mice (9-11 wk old) were anesthetized and BALF was collected by instilling 500 μL PBS 3 times through the tracheal cannula into the lungs on day 2, 7 and 21. Cells were collected from BALF by centrifugation (4 °C, 400 *g*, 5 min) and total numbers and cell differentiation were counted using an automated cell counter (Countess II FL Automated Cell Counter; Thermo Fisher Scientific, Waltham, MA, USA) and cytospin technique.

Detection of NETs in BAL cells

Collected cells from BAL were incubated with RBC lysis solution (Miltenyi Biotec, Bergisch Gladbach, Germany) according to manufacturer's instructions. After counting, 1×10^5 cells per well were seeded onto 4-well chamber slides (Thermo Fisher Scientific). Cells were fixed in 4 % (wt/vol) paraformaldehyde for 10 min, blocked with Block Ace (Dainihon Pharmaceutical Co., Tokyo, Japan) for 30 min, and incubated with primary antibodies at 4 °C overnight. Cells were incubated with secondary antibodies for 60 min, mounted with Vectashield mounting medium with DAPI (4′-6-diamidino-2-phenylindole dihydrochloride) (Vector Laboratories, Inc., Burlingame, CA, USA), and visualized using a confocal microscope (Fluoview FV 10i; Olympus, Tokyo, Japan).

Isolation of mouse neutrophils and induction of NETs in vitro

Resected bilateral femur and tibia were cut at both edges, and flushed with RPMI-1640 medium (Sigma, St. Louis, MO, USA) supplemented with penicillin-streptomycin-glutamine and fetal bovine serum (Gibco BRL, Tokyo, Japan). After RBC lysis, cells suspended in PBS were separated using Ficoll paque PLUS (GE Healthcare, Tokyo, Japan), and neutrophils were collected in the bottom layer. The number and differentiation of cells were evaluated using the cytospin method.

Collected neutrophils were seeded onto 4-well chamber slides at concentration of 6.25×10^5 cells/mL. After 2.5 h incubation at 37 °C in 5 % CO_2 with ionomycin (4 μM; Wako, Tokyo, Japan), BLM (50 μg/mL), Cl-amidine (100 μM; Cayman Chemical, Ann Arbor, MI, USA), and DNAse-1 (10 U/mL; Wako), cells were fixed, blocked, and incubated with primary antibodies at 4 °C overnight and finally with secondary antibodies for 60 min at 25 °C. After mounting with DAPI, NETs were observed under a confocal microscope (Olympus).

Results

BLM instillations induced NETs in the lungs of mice

To examine the existence of NETs in BLM-induced lung fibrosis, we evaluated the expression of NETs in BAL cells of wild-type (WT) mice 2, 7, and 21 d after instillations of BLM or vehicle. We confirmed that BLM induced lung fibrosis with the alterations of the total cell number and differentiation of BAL cells (Figure S1A, S1B). As shown in Figure 1A, NETs were clearly induced by BLM instillations. The percentage of NETs in neutrophils peaked at day 2 and gradually declined over time (Figure 1B). Existence of NETs was observed in the interstitial space only in the BLM group on day 2 (Figure 1C). Thus, these findings suggested that BLM instillations were responsible for inducing the expression of NETs in the lungs of mice.

BLM-induced NETs depended on activity of PADs both in vivo and in vitro

As activation by PAD proteins plays an important role in the formation of NETs, we assessed whether Cl-amidine, a pan-PAD inactivator, could suppress BLM-induced NETs both *in vivo* and *in vitro*. The existence of BLM-induced NETs in BAL cells was suppressed *in vivo* by Cl-amidine (Figure 2A). After BLM induction, the percentage of NETs in BAL neutrophils in the Cl-amidine treated group was significantly lower compared with that in the vehicle group ($p < 0.01$; Figure 2B). Meanwhile, the total cell numbers and differentiations of BAL cells were similar between the groups (Figure 2C). After BLM instillations, NETs expression in the interstitial space in the Cl-amidine treated group was suppressed compared with that in the vehicle group (Figure 2D). Consistent with a previous study (26), *in vitro* administration of BLM as well as ionomycin calcium, a known inducer of NETs, directly induced NETs in blood neutrophils. On the other hand, BLM-induced NETs were diminished by DNAse-1, a known degrader of NETs. The percentage of BLM-induced NETs was significantly decreased by Cl-amidine but not by vehicle (BLM + vehicle vs. BLM + Cl-amidine; $p = 0.03$) (Figure 2E, 2F). Thus, BLM induced the expression of NETs both *in vivo* and *in vitro* and their formation depended on the activity of PAD.

Deficiency of PAD4 suppressed BLM-induced NETs and expression of inflammatory genes

As PADs are composed of 5 types of enzymes, PAD1, 2, 3, 4 and 6, of which PAD4 is considered to contribute to the induction of NETs (17, 18), we attempted to verify the role of PAD4 deficiency in BLM-induced NETs using PAD4-KO mice. WT and PAD4-KO mice were intratracheally administered BLM or vehicle and examined on day 2. The numbers and cell differentiations of BAL cells were not different between the WT and PAD4-KO groups (Figure 3A). However, the expression of NETs in the BAL cells of PAD4-KO mice was suppressed compared with that of WT mice (Figure 3B). After BLM instillations, the percentage of NETs in BAL neutrophils of PAD4-KO mice was significantly lower compared with that of WT mice ($p < 0.01$; Figure 3C). Furthermore, the expression of NETs was suppressed in the lung parenchyma of PAD4-KO mice compared with WT mice (Figure 3D). Regarding quantitative real-time polymerase chain reaction (qRT-PCR) analyses, in the BLM groups, the mRNA expression levels of interleukin-6 (*Il-6*) and interferon γ (*Ifn-γ*) of PAD4-KO mice were significantly lower compared with those of WT mice (*Il-6*: $p = 0.02$, *Ifn-γ*: $p = 0.03$); moreover, the mRNA level of tumor necrosis factor α (*Tnf-α*) of PAD4-KO mice showed a decreased expression trend compared to that of WT mice (Figure 3E). Thus, these results indicated that deletion of PAD4 alleviated BLM-induced formation of NETs in the lungs and expression of inflammatory genes.

Deficiency of PAD4 suppressed BLM-induced pulmonary fibrosis and expression of fibrosis-related genes

Next, we sought to examine whether deficiency of PAD4 could alleviate BLM-induced lung fibrosis. We intratracheally administered BLM or vehicle to WT and PAD4-KO mice and examined their lungs on day 21. Figure 4A shows the time course of the weight changes in mice until day 21. On day 2 and 4, the weight loss

in the BLM groups of PAD4-KO mice was significantly smaller than that of WT mice (day 2: $p < 0.01$, day 4: $p < 0.01$). PAD4-KO may not affect the survival rates since those in BLM-administered WT and PAD4-KO mice were similar (WT + BLM vs. PAD4-KO + BLM; 65 % vs. 65 %, $p = 0.91$; Figure 4B). Masson's trichrome staining of lung tissue sections revealed that the extent of pulmonary fibrosis and the fibrosis scores of the lungs of PAD4-KO mice seemed to be milder compared with those of WT mice after BLM instillations ($p = 0.01$; Figure 4C, 4D). Likewise, the collagen loads of the lungs of PAD4-KO mice were also significantly slight compared with those of WT mice lungs ($p < 0.01$; Figure 4E). The mRNA expression levels of fibrosis-related genes, including collagen type I alpha 1 chain (*Col1a1*), elastin (*Eln*), fibronectin 1 (*Fn1*), connective tissue growth factor (*Ctgf*), and fibroblast growth factor 2 (*Fgf2*) of PAD4-KO mice group were significantly lower compared to WT mice group after BLM instillations (*Col1a1*: $p < 0.01$, *Eln*: $p < 0.01$, *Fn1*: $p = 0.02$, *Ctgf*: $p = 0.02$, *Fgf2*: $p < 0.01$). Additionally, the mRNA expression levels of smooth muscle alpha actin (*Acta2*) and transforming growth factor β1 (*Tgfβ1*) of PAD4-KO mice tended to be lower than those of WT mice after BLM induction (Figure 4F). These findings suggested that inhibition of PAD4 suppressed BLM-induced pulmonary fibrosis and the expression of fibrosis-related genes.

Deficiency of PAD4 alleviated the alteration of the structural cell profiles of lungs induced by BLM instillations

Based on previous studies showing that NETs were able to induce lung epithelial and endothelial cell death and promote transition of lung fibroblasts to myofibroblasts (26, 30), we used flow cytometry analysis to assess the alterations of the structural cell profiles of lungs in WT and PAD4-KO mice during the pulmonary fibrosing period (Figure 5A-5E). We defined type-I (AEC-I), and type-II (AEC-II) alveolar epithelial cells, pulmonary vascular endothelial cells (PVECs), and α-SMA positive mesenchymal cells as $AQP5^{+}/CD31^{-}/CD45^{-}$ cells, $SP\text{-}C^{+}/CD31^{-}/CD45^{-}$ cells, $CD31^{+}/CD45^{-}$ cells, and $\alpha\text{-}SMA^{+}/CD31^{-}/CD45^{-}$ cells, respectively. Compared with the vehicle group, the numbers of total lung cells and α-SMA positive mesenchymal cells of the BLM group in WT mice were significantly greater (total lung cells: $p = 0.04$, α-SMA positive mesenchymal cells: $p = 0.04$; Figure 5A, 5E), whereas the numbers of AEC-I, AEC-II, and PVECs were significantly smaller (AEC-I: $p = 0.04$, AEC-II: $p = 0.04$, PVECs: $p = 0.04$; Figure 5B-5D). However, the numbers of total lung cells, AEC-I, AEC-II, PVECs, and α-SMA positive mesenchymal cells between the vehicle and BLM group in PAD4-KO mice did not show significant differences (Figure 5A-5E). Thus, the inhibition of PAD4 was able to alleviate the decrease of alveolar epithelial cells and PVECs and increase of α-SMA positive mesenchymal cells during fibrosis.

PAD4 in hematopoietic cells contributed to the development of BLM-induced pulmonary fibrosis in WT mice

To verify the contribution of the function of PAD4 enzyme in hematopoietic cells versus lung structural cells in the development of BLM-induced pulmonary fibrosis, we generated radiation-induced bone marrow (BM) chimeric mice. First, we examined whether the BM of PAD4-KO mice could be engrafted in WT mice. Namely, irradiated green fluorescent protein (GFP) mice were infused with BM cells from PAD4-KO mice. The percentage of GFP negative cells in the population of peripheral white blood cells of GFP mice was analyzed overtime by flow cytometry (Figure 6A). The mean observed percentage was over 90 % after the 5th wk (means ± SEM, 4 wk: 88.7 ± 2.1, 5 wk: 90.9 ± 1.3, 6 wk: 92.3 ± 1.4, 7 wk: 93.1 ± 1.6, 8 wk: 94.1 ± 1.3, respectively), indicating that the graft of BM cells from PAD4-KO mice was well established.

Finally, we evaluated the extent of BLM-induced pulmonary fibrosis in the chimeric mice. The flow scheme of the experiment is shown in Figure 6B. Masson's trichrome staining of lung tissue sections revealed that the extent of BLM-induced pulmonary fibrosis and fibrosis scores in WT mice transplanted with BM cells from PAD4-KO mice were significantly milder compared with those in WT mice infused with BM cells from WT mice ($p = 0.01$; Figure 6C, 6D). Thus, this result suggested that the function of PAD4 in hematopoietic cells contributed to the development of BLM-induced pulmonary fibrosis.

243 **Discussion**
244
245 In this study, we first identified that NETs are present in the lungs of mice undergoing experimental lung
246 fibrosis. Following induction with BLM, NETs were mainly expressed during the inflammatory period and
247 were observed in the alveolar and interstitial space. Second, we demonstrated that BLM-induced NETs
248 depended on the activation of PAD proteins both *in vivo* and *in vitro*. Third, deficiency of PAD4 led to reduced
249 formation of NETs and pulmonary fibrosis, as well as prevented the decrease of alveolar epithelial and
250 endothelial cell numbers and increase of α-SMA positive mesenchymal cell numbers. Finally, we found that
251 adoptive transfer of hematopoietic cells from PAD4-KO but not from WT resolved lung fibrosis in WT mice,
252 suggesting that the expression of PAD4 in hematopoietic cells was involved in the development of BLM-
253 induced lung fibrosis. Collectively, these data suggested the important role of PAD4 in the BLM-induced
254 formation of NETs and development of lung fibrosis.
255
256 This is the first study demonstrating that expression of NETs was observed in BAL cells and the lung
257 parenchymal space, particularly during the inflammatory period in an experimental lung fibrosis model. We
258 defined NETs as rounded-up cells or web-like structures accompanied with nuclear, citH3 and neutrophilic
259 markers (Ly6G or NE) according to previous reports (13, 14). The formation of NETs, which functions as
260 part of the innate immune defense, is a process of mixing cellular nuclear, cytosolic proteins and chromatin,
261 which are then released into the extracellular space (13, 14), contributing in trapping and killing bacteria.
262 Meanwhile, excessive expression of NETs has been reported to cause multiple organ damages under
263 infectious conditions, and to also contribute to the etiologies of non-infectious diseases by inducing direct
264 cell damage, inflammation, and vascular occlusion (15, 16, 20-24). The current study adds BLM-induced
265 lung fibrosis to the list of disease models involving the function of NETs. Coincident with the timing of
266 elevation of the number of neutrophils in BALF, expression of NETs was mostly observed in the lung,
267 suggesting that inflammation induced by BLM promoted the migration of neutrophils and formation of
268 NETs in the lung.
269
270 Although a former study showed that NETs were induced by BLM *in vitro* (26), the mechanisms by which
271 BLM was able to promote formation of NETs both *in vivo* and *in vitro* have been unclear. NETs were shown
272 to be induced by various stimulants, such as PMA, ionomycin calcium, LPS, various types of bacteria,
273 production of reactive oxygen species (ROS) by NADPH oxidase, and cytokines (e.g., IL-8 and tumor necrosis
274 factor-α (TNF-α)) (14, 16, 17). Citrullination is the posttranslational deamination of arginine residues to
275 citrullines, catalyzed by PADs (17, 18). Histone citrullination has been reported to promote the formation of
276 NETs by inducing chromatin decondensation. Meanwhile, activation of NE/myeloperoxidase (MPO) or
277 autophagy were proposed to regulate the formation of NETs, as well as histone citrullination by PADs (31, 32).
278 Among the above reported stimuli, ROS is known to be significantly produced in the lungs following BLM
279 instillation (33). The formation of NETs induced by the production of ROS has been shown to be mediated by
280 the activation of PADs (17). Here, we clearly showed that the BLM-induced NETs were reduced following
281 administration of a PAD inhibitor *in vivo*. In addition, we demonstrated that BLM directly induced neutrophils
282 to form NETs *in vitro* in a PAD dependent manner.
283
284 PADs consist of 5 types of enzymes, namely PAD1, 2, 3, 4 and 6 (17, 18). Noted, PAD2 and PAD4 are present
285 in neutrophils and their roles in the formation of different type of NETs has been questioned (34). Although
286 PAD2 is known to be present in NETs and contribute to histone citrullination, a recent study demonstrated that
287 PAD2 was required for citrullination but was not essential for formation of NETs in a TNFα-induced arthritis
288 model (35). Similarly, PAD4-independent formation of NETs regulated by the NE/MPO or autophagy pathway

289 has also been reported (31, 32). On the contrary, activation of PAD4 was shown to be required for the
290 production of NETs induced by various other stimuli (34, 35). Thus, as the function of PAD4 appeared to be
291 considered rather important in the formation of BLM-induced NETs, we decided in this study to analyze a role
292 of PAD4 using PAD4-KO mice.
293
294 We demonstrated that the BLM-induced NETs in BAL cells and lung parenchyma were PAD4 dependent.
295 Interestingly, the numbers and cell differentiations of BAL cells were not different between the WT and PAD4-
296 KO groups. Meanwhile, the increased gene expression of inflammatory mediators induced by BLM was
297 suppressed by deficiency of PAD4. These results suggested that depletion of PAD4 might not affect the
298 accumulation of inflammatory cells itself, but suppress the formation of NETs and the expression of
299 inflammatory mediator genes in the lungs during the acute phase of lung injury induced by BLM. During the
300 acute phase (day 2 and 4), the weight losses in the BLM group of PAD4-KO mice were suppressed compared
301 with those of WT mice. However, there were no significant differences observed in the weight of mice between
302 both groups in later periods, suggesting that deficiency of PAD4 might contribute to the reduction of systemic
303 inflammation in early phase.
304
305 Although the survival rate was similar between WT and PAD4-KO mice, the degree of BLM-induced
306 pulmonary fibrosis in PAD4-KO mice was significantly suppressed compared with WT mice. Similarly, the
307 gene expression of fibrosis-related mediators (*Col1a1*, *Eln*, *Fn1*, *Ctgf*, and *Fgf2*) was significantly
308 suppressed in PAD4-KO mice after BLM induction. Several former studies have demonstrated that NETs
309 were associated with organ fibrosis. Martinod et al. reported that age-related pulmonary and cardiac fibrosis
310 was suppressed in PAD4-KO mice, as a lack of NETs attenuated the accumulation of platelets and
311 production of TGFβ, a potent fibrosis driver, leading to the resolution of the fibrosis (29). Similarly, Sorvillo
312 N. et al. reported that interaction of NETs with the von Willebrand factor and platelets might contribute to
313 tissue fibrosis during ischemic/reperfusion injury (36). Likewise, vascular damage and endothelial to
314 mesenchymal transition (EndMT) by NETs were proposed to contribute to kidney fibrosis (37). Additionally,
315 NE, a protease released along with NETs maintaining its activity, was shown to be directly associated with
316 BLM-induced mice pulmonary fibrosis (8). Other components of NETs, such as LL-37 (Cathelicidin),
317 S100A8, S100A9 and defensin, were also reported to be associated with the process of tissue fibrosis (38-
318 40). Additionally, the gene expression of *Ctgf*, *Fgf2*, and *TGFβ1* have been known to constitute key factors
319 of pulmonary fibrogenesis in IPF and BLM-induced pulmonary fibrosis (2-4, 41). Our current observation
320 has been in agreement with these previous studies. Thus, we speculated that during a lung injury reduction of
321 NETs formation by deficiency of PAD4 might prevent BLM-induced lung fibrosis in the current study.
322
323 Reduction in the population of alveolar epithelial and endothelial cells with parallel increase in that of α-SMA
324 positive mesenchymal cells, which are significantly involved in pulmonary fibrogenesis, have been commonly
325 observed in both human and mice (2, 42, 43). Thus, we examined the changes in the populations of lung tissue
326 cells *in vivo*. Based on the finding from a previous research that alveolar epithelial and endothelial cells
327 decreased and α-SMA positive mesenchymal cells increased on day 14 after BLM instillation (44), we
328 conducted a flow cytometric assay on day 14. Consistent with the previous study, the numbers of epithelial
329 and endothelial cells decreased, whereas those of α-SMA positive mesenchymal cells increased in WT mice.
330 Interestingly, deficiency of PAD4 prevented both the decrease in the number of alveolar and endothelial cells
331 and the increase in the number of α-SMA mesenchymal cells. Although the precise mechanisms above are
332 unclear, several studies have demonstrated that NETs have detrimental effects on tissue cell components
333 related to the fibrotic process. For example, NETs are known to cause pulmonary vascular endothelial cell and
334 alveolar epithelial cell death in an ARDS model (30). In addition, NETs were reported to induce EndMT

associated with kidney fibrosis (37). Furthermore, NETs promoted differentiation of lung fibroblasts to a myofibroblast phenotype in culture, increasing the expression of *Ctgf*, production of collagen and proliferation/migration of fibroblasts (26). Thus, we speculated that loss of NETs according to deficiency of PAD4 might have a protective effect against alterations of tissue cell components during fibrosis.

Although the PAD4 enzyme mainly exists in neutrophils, expression of PAD4 mRNA has been weakly detected in systemic organs, such as brain, lung, heart, liver, spleen, kidney and skin (17, 18, 29). Thus, to verify whether the anti-fibrotic effect associated with the deficiency of PAD4 is due to hematopoietic cells or organ structural cells, we performed experiments using irradiated, BM chimeric mice reconstituted with PAD4-KO or WT hematopoietic cells. First, we confirmed that hematopoietic cells from PAD4-KO mice were successfully engrafted in WT mice. Next, we demonstrated that BLM-induced lung fibrosis was prevented in mice expressing PAD4 on radioresistant structural cells, but not on hematopoietic cells. In contrast, mice expressing PAD4 on both radioresistant structural cells and hematopoietic cells, exhibited fibrotic changes in their lungs. These data suggested the importance of PAD4 expressed on hematopoietic cells in the development of BLM-induced pulmonary fibrosis.

The present study has several implications as there have been reports demonstrating the relationship between NETs and human pulmonary fibrosis. The existence of NETs was observed in pulmonary fibrosis, in which expression of fibrotic mediators was identified neighboring NETs (26). Additionally, the increase of serum cell free DNA (cfDNA) has been demonstrated in IPF, with increased serum cfDNA levels being useful in distinguishing patients with IPF from other patients (45). Aging and cellular senescence have been considered as key factors in the pathogenesis of IPF (46) and PAD4-deficient mice were shown to exhibit a reduction of age-related lung fibrosis (29). In addition, patients with PM/DM who had elevated numbers of components of NETs and dysfunction of the degrading enzyme of NETs tended to exhibit complicated ILD (28). In both patients with IPF and rheumatoid arthritis with ILD, the mRNA levels of PAD4 in BAL cells were significantly increased compared with healthy controls (47). The results of this study suggested a role for PAD4 in the induction of NETs and the pathogenesis of lung fibrosis.

This study has some limitations. First, there might exist unknown mechanisms regarding formation of NETs except for the one induced by activation of PAD4. In the current study, BLM-induced NETs were not completely inhibited in PAD4-KO mice. As mentioned above, previous studies proposed that besides activation of PAD4, activation of NE/MPO and autophagy might contribute to the formation of NETs (31, 32). Although our results demonstrated that BLM-induced NETs were dominantly regulated by PAD4, further studies are required to elucidate the precise mechanisms of the formation of NETs in pulmonary fibrosis. Second, the role of NETs in BLM-induced fibrosis has not been fully elucidated. Apart from its role in the formation of NETs, PAD4 is known to be involved in gene expression by regulating histone methylation (48). Thus, we could not exclude the possibility that there could been contributing changes in the expression of genes in the organ tissue itself caused by the deficiency of PAD4 (29). We also demonstrated that pulmonary fibrosis was significantly reduced following deletion of PAD4 in hematopoietic cells. However, we did not perform experiments using BM chimeric mice reconstituted with PAD4-KO or WT hematopoietic cells in PAD4-KO mice. Thus, the effect of the deficiency of PAD4 in structural cells in lung fibrosis has not been elucidated. However, PAD4 is only weakly expressed in lung tissues (29). As another group proposed a role for NETs in organ fibrosis and concluded that PAD4 could regulate age-related organ fibrosis and dysfunction, we speculated that NETs were regulated by PAD4 and augmented BLM-induced fibrosis. Third, BLM does not mimic human IPF (41, 49), as BLM-induced pulmonary fibrosis is deeply associated with inflammation. Compared to human IPF, although the early molecular events of BLM-induced pulmonary fibrosis resemble

IPF, reversible fibrosis and inflammation preceding fibrosis are different from IPF (41). However, BLM-induced pulmonary fibrosis is considered "the best-characterized animal model available for preclinical testing" according to the American international society (49).

In summary, we demonstrated that NETs were induced by BLM instillation. The deficiency of PAD4 was able to ameliorate BLM-induced NETs and fibrosis in the lung, which are associated with reduced levels of inflammation and expression of fibrosis associated genes, including *Il-6*, *Tnf-α*, *Ctgf*, *Fgf2*, and *Col1a1*. In addition, we elucidated the role of the deficiency of PAD4 in the proportions of lung structural cells during lung fibrosis. Finally, we demonstrated that PAD4 in hematopoietic cells plays an important role in the development of pulmonary fibrosis. Our results suggested that reduction of NETs by inhibition of PAD4 might be a promising strategy for the treatment of pulmonary fibrosis.

394 **References**
395
396 1. Raghu G, Remy-Jardin M, Myers JL, Richeldi L, Ryerson CJ, Lederer DJ, Behr J, Cottin V, Danoff SK,
397 Morell F, Flaherty KR, Wells A, Martinez FJ, Azuma A, Bice TJ, Bouros D, Brown KK, Collard HR, Duggal
398 A, Galvin L, Inoue Y, Jenkins RG, Johkoh T, Kazerooni EA, Kitaichi M, Knight SL, Mansour G, Nicholson
399 AG, Pipavath SNJ, Buendía-Roldán I, Selman M, Travis WD, Walsh S, Wilson KC; American Thoracic
400 Society, European Respiratory Society, Japanese Respiratory Society, and Latin American Thoracic Society.
401 Diagnosis of Idiopathic Pulmonary Ffibrosis. An Official ATS/ERS/JRS/ALAT Clinical Practice Guideline.
402 *Am J Respir Crit Care Med* 2018;198:e44-e68.
403 2. Knudsen L, Ruppert C, Ochs M. Tissue remodelling in pulmonary fibrosis. *Cell Tissue Res* 2017;367:607-
404 626.
405 3. Kolahian S, Fernandez IE, Eickelberg O, Hartl D. Immune Mechanisms in Pulmonary Fibrosis. *Am J Respir*
406 *Cell Mol Biol* 2016;55:309-322.
407 4. Desai O, Winkler J, Minasyan M, Herzog EL. The Role of Immune and Inflammatory Cells in Idiopathic
408 Pulmonary Fibrosis. *Front Med (Lausanne)* 2018;5:43.
409 5. Fingerlin TE, Murphy E, Zhang W, Peljto AL, Brown KK, Steele MP, Loyd JE, Cosgrove GP, Lynch D,
410 Groshong S, Collard HR, Wolters PJ, Bradford WZ, Kossen K, Seiwert SD, du Bois RM, Garcia CK, Devine
411 MS, Gudmundsson G, Isaksson HJ, Kaminski N, Zhang Y, Gibson KF, Lancaster LH, Cogan JD, Mason WR,
412 Maher TM, Molyneaux PL, Wells AU, Moffatt MF, Selman M, Pardo A, Kim DS, Crapo JD, Make BJ, Regan
413 EA, Walek DS, Daniel JJ, Kamatani Y, Zelenika D, Smith K, McKean D, Pedersen BS, Talbert J, Kidd RN,
414 Markin CR, Beckman KB, Lathrop M, Schwarz MI, Schwartz DA. Genome-wide association study identifies
415 multiple susceptibility loci for pulmonary fibrosis. *Nat Genet* 2013;45:613-620.
416 6. Nathan C. Neutrophils and immunity: challenges and opportunities. *Nat Rev Immunol* 2006;6:173-182.
417 7. Wang J. Neutrophils in tissue injury and repair. *Cell Tissue Res* 2018;371:531-539.
418 8. Gregory AD, Kliment CR, Metz HE, Kim KH, Kargl J, Agostini BA, Crum LT, Oczypok EA, Oury TA,
419 Houghton AM. Neutrophil elastase promotes myofibroblast differentiation in lung fibrosis. *J Leukoc Biol*
420 2015;98:143-152.
421 9. Pesci A, Ricchiuti E, Ruggiero R, De Micheli A. Bronchoalveolar lavage in idiopathic pulmonary fibrosis:
422 What does it tell us? *Respir Med* 2010;104 Suppl 1:S70-73.
423 10. Kinder BW, Brown KK, Schwarz MI, Ix JH, Kervitsky A, King TE, Jr. Baseline BAL neutrophilia predicts
424 early mortality in idiopathic pulmonary fibrosis. *Chest* 2008;133:226-232.
425 11. Emura I, Usuda H, Togashi K, Satou K. Minute lesions of alveolar damage in lungs of patients with stable
426 idiopathic pulmonary fibrosis. *Histopathology* 2015;67:90-95.
427 12. Guiot J, Moermans C, Henket M, Corhay JL, Louis R. Blood Biomarkers in Idiopathic Pulmonary Fibrosis.
428 *Lung* 2017;195:273-280.
429 13. Brinkmann V, Reichard U, Goosmann C, Fauler B, Uhlemann Y, Weiss DS, Weinrauch Y, Zychlinsky A.
430 Neutrophil extracellular traps kill bacteria. *Science* 2004;303:1532-1535.
431 14. Fuchs TA, Abed U, Goosmann C, Hurwitz R, Schulze I, Wahn V, Weinrauch Y, Brinkmann V, Zychlinsky
432 A. Novel cell death program leads to neutrophil extracellular traps. *J Cell Biol* 2007;176(2):231-241.
433 15. Jorch SK, Kubes P. An emerging role for neutrophil extracellular traps in noninfectious disease. *Nat Med*
434 2017;23:279-287.
435 16. Pruchniak MP, Kotula I, Manda-Handzlik A. Neutrophil extracellular traps (Nets) impact upon
436 autoimmune disorders. *Cent Eur J Immunol* 2015;40:217-224.
437 17. Rohrbach AS, Slade DJ, Thompson PR, Mowen KA. Activation of PAD4 in NET formation. *Front*
438 *Immunol* 2012;3:360.
439 18. Wang S, Wang Y. Peptidylarginine deiminases in citrullination, gene regulation, health and pathogenesis.

Biochim Biophys Acta 2013;1829:1126-1135.
19. Czaikoski PG, Mota JM, Nascimento DC, Sonego F, Castanheira FV, Melo PH, Scortegagna GT, Silva RL, Barroso-Sousa R, Souto FO, Pazin-Filho A, Figueiredo F, Alves-Filho JC, Cunha FQ. Neutrophil Extracellular Traps Induce Organ Damage during Experimental and Clinical Sepsis. *PLoS One* 2016;11:e0148142.
20. Martinod K, Wagner DD. Thrombosis: tangled up in NETs. *Blood* 2014;123:2768-2776.
21. Caudrillier A, Kessenbrock K, Gilliss BM, Nguyen JX, Marques MB, Monestier M, Toy P, Werb Z, Looney MR. Platelets induce neutrophil extracellular traps in transfusion-related acute lung injury. *J Clin Invest* 2012;122:2661-2671.
22. Cools-Lartigue J, Spicer J, McDonald B, Gowing S, Chow S, Giannias B, Bourdeau F, Kubes P, Ferri L. Neutrophil extracellular traps sequester circulating tumor cells and promote metastasis. *J Clin Invest* 2013: 67484.
23. Wong SL, Demers M, Martinod K, Gallant M, Wang Y, Goldfine AB, Kahn CR, Wagner DD. Diabetes primes neutrophils to undergo NETosis, which impairs wound healing. *Nat Med* 2015;21:815-819.
24. Warnatsch A, Ioannou M, Wang Q, Papayannopoulos V. Inflammation. Neutrophil extracellular traps license macrophages for cytokine production in atherosclerosis. *Science* 2015;349:316-320.
25. Wright TK, Gibson PG, Simpson JL, McDonald VM, Wood LG, Baines KJ. Neutrophil extracellular traps are associated with inflammation in chronic airway disease. *Respirology* 2016;21:467-475.
26. Chrysanthopoulou A, Mitroulis I, Apostolidou E, Arelaki S, Mikroulis D, Konstantinidis T, Sivridis E, Koffa M, Giatromanolaki A, Boumpas DT, Ritis K, Kambas K. Neutrophil extracellular traps promote differentiation and function of fibroblasts. *J Pathol* 2014;233:294-307.
27. Martinez-Aleman SR, Campos-Garcia L, Palma-Nicolas JP, Hernandez-Bello R, Gonzalez GM, Sanchez-Gonzalez A. Understanding the Entanglement: Neutrophil Extracellular Traps (NETs) in Cystic Fibrosis. *Front Cell Infect Microbiol* 2017;7:104.
28. Zhang S, Shu X, Tian X, Chen F, Lu X, Wang G. Enhanced formation and impaired degradation of neutrophil extracellular traps in dermatomyositis and polymyositis: A potential contributor to interstitial lung disease complications. *Clin Exp Immunol* 2014;177:134-141.
29. Martinod K, Witsch T, Erpenbeck L, Savchenko A, Hayashi H, Cherpokova D, Gallant M, Mauler M, Cifuni SM, Wagner DD. Peptidylarginine deiminase 4 promotes age-related organ fibrosis. *J Exp Med* 2017;214:439-458.
30. Saffarzadeh M, Juenemann C, Queisser MA, Lochnit G, Barreto G, Galuska SP, Lohmeyer J, Preissner KT. Neutrophil extracellular traps directly induce epithelial and endothelial cell death: A predominant role of histones. *PLoS One* 2012;7:e32366.
31. Skendros P, Mitroulis I, Ritis K. Autophagy in Neutrophils: From Granulopoiesis to Neutrophil Extracellular Traps. *Front Cell Dev Biol* 2018;6:109.
32. Papayannopoulos V, Metzler KD, Hakkim A, Zychlinsky A. Neutrophil elastase and myeloperoxidase regulate the formation of neutrophil extracellular traps. *J Cell Biol* 2010;191:677-691.
33. Cheresh P, Kim SJ, Tulasiram S, Kamp DW. Oxidative stress and pulmonary fibrosis. *Biochim Biophys Acta* 2013;1832:1028-1040.
34. Holmes CL, Shim D, Kernien J, Johnson CJ, Nett JE, Shelef MA. Insight into Neutrophil Extracellular Traps through Systematic Evaluation of Citrullination and Peptidylarginine Deiminases. *J Immunol Res* 2019;2019:2160192.
35. Bawadekar M, Shim D, Johnson CJ, Warner TF, Rebernick R, Damgaard D, Nielsen CH, Pruijn GJM, Nett JE, Shelef MA. Peptidylarginine deiminase 2 is required for tumor necrosis factor alpha-induced citrullination and arthritis, but not neutrophil extracellular trap formation. *J Autoimmun* 2017;80:39-47.
36. Sorvillo N, Cherpokova D, Martinod K, Wagner DD. Extracellular DNA NET-Works with Dire Consequences for Health. *Circ Res* 2019;125:470-488.

37. Salazar-Gonzalez H, Zepeda-Hernandez A, Melo Z, Saavedra-Mayorga DE, Echavarria R. Neutrophil Extracellular Traps in the Establishment and Progression of Renal Diseases. *Medicina (Kaunas)* 2019;55:E431.
38. Takahashi T, Asano Y, Nakamura K, Yamashita T, Saigusa R, Ichimura Y, Toyama T, Taniguchi T, Yoshizaki A, Tamaki Z, Tada Y, Sugaya M, Kadono T, Sato S. A potential contribution of antimicrobial peptide LL-37 to tissue fibrosis and vasculopathy in systemic sclerosis. *Br J Dermatol* 2016;175:1195-1203.
39. Zhong A, Xu W, Zhao J, Xie P, Jia S, Sun J, Galiano RD, Mustoe TA, Hong SJ. S100A8 and S100A9 Are Induced by Decreased Hydration in the Epidermis and Promote Fibroblast Activation and Fibrosis in the Dermis. *Am J Pathol* 2016;186:109-122.
40. Mukae H, Iiboshi H, Nakazato M, Hiratsuka T, Tokojima M, Abe K, Ashitani J, Kadota J, Matsukura S, Kohno S. Raised plasma concentrations of alpha-defensins in patients with idiopathic pulmonary fibrosis. *Thorax* 2002;57:623-628.
41. Della Latta V, Cecchettini A, Del Ry S, Morales MA. Bleomycin in the setting of lung fibrosis induction: From biological mechanisms to counteractions. *Pharmacol Res* 2015;97:122-130.
42. Williamson JD, Sadofsky LR, Hart SP. The pathogenesis of bleomycin-induced lung injury in animals and its applicability to human idiopathic pulmonary fibrosis. *Exp Lung Res* 2015;41(2):57-73.
43. Bagnato G, Harari S. Cellular interactions in the pathogenesis of interstitial lung diseases. *Eur Respir Rev* 2015;24:102-114.
44. Tsukui T, Ueha S, Abe J, Hashimoto S, Shichino S, Shimaoka T, Shand FH, Arakawa Y, Oshima K, Hattori M, Inagaki Y, Tomura M, Matsushima K. Qualitative rather than quantitative changes are hallmarks of fibroblasts in bleomycin-induced pulmonary fibrosis. *Am J Pathol* 2013;183:758-773.
45. Travis WD, Costabel U, Hansell DM, King TE, Jr., Lynch DA, Nicholson AG, Ryerson CJ, Ryu JH, Selman M, Wells AU, Behr J, Bouros D, Brown KK, Colby TV, Collard HR, Cordeiro CR, Cottin V, Crestani B, Drent M, Dudden RF, Egan J, Flaherty K, Hogaboam C, Inoue Y, Johkoh T, Kim DS, Kitaichi M, Loyd J, Martinez FJ, Myers J, Protzko S, Raghu G, Richeldi L, Sverzellati N, Swigris J, Valeyre D; ATS/ERS Committee on Idiopathic Interstitial Pneumonias. An official American Thoracic Society/European Respiratory Society statement: Update of the international multidisciplinary classification of the idiopathic interstitial pneumonias. *Am J Respir Crit care Med* 2013;188:733-748.
46. Schafer MJ, White TA, Iijima K, Haak AJ, Ligresti G, Atkinson EJ, Oberg AL, Birch J, Salmonowicz H, Zhu Y, Mazula DL, Brooks RW, Fuhrmann-Stroissnigg H, Pirtskhalava T, Prakash YS, Tchkonia T, Robbins PD, Aubry MC, Passos JF, Kirkland JL, Tschumperlin DJ, Kita H, LeBrasseur NK. Cellular senescence mediates fibrotic pulmonary disease. *Nat Commun* 2017;8:14532.
47. Samara KD, Trachalaki A, Tsitoura E, Koutsopoulos AV, Lagoudaki ED, Lasithiotaki I, Margaritopoulos G, Pantelidis P, Bibaki E, Siafakas NM, Tzanakis N, Wells AU, Antoniou KM. Upregulation of citrullination pathway: From Autoimmune to Idiopathic Lung Fibrosis. *Respir Res* 2017;18:218.
48. Wang Y, Wysocka J, Sayegh J, Lee YH, Perlin JR, Leonelli L, Sonbuchner LS, McDonald CH, Cook RG, Dou Y, Roeder RG, Clarke S, Stallcup MR, Allis CD, Coonrod SA. Human PAD4 regulates histone arginine methylation levels via demethylimination. *Science* 2004;306:279-283.
49. Jenkins RG, Moore BB, Chambers RC, Eickelberg O, Konigshoff M, Kolb M, Laurent GJ, Nanthakumar CB, Olman MA, Pardo A, Selman M, Sheppard D, Sime PJ, Tager AM, Tatler AL, Thannickal VJ, White ES; ATS Assembly on Respiratory Cell and Molecular Biology. An Official American Thoracic Society Workshop Report: Use of Animal Models for the Preclinical Assessment of Potential Therapies for Pulmonary Fibrosis. *Am J Respir Cell Mol Biol* 2017;56:667-679.

529 **Figure legends**
530
531 Figure 1. Bleomycin (BLM) instillations induce neutrophil extracellular traps (NETs) in the lungs of mice.
532 Wild-type (WT) mice received BLM or vehicle by intratracheal instillations. (A) Representative
533 immunofluorescent staining of bronchoalveolar lavage (BAL) cells for DAPI (blue), Ly6G (green), and
534 citrullinated histone H3 (citH3; red) on day 2 after BLM or vehicle instillations. (B) The percentage of NETs
535 in BAL neutrophils on day 2, 7 and 21 after BLM (closed bar) or vehicle (open bar) instillations. Results for
536 each group are expressed as means ± SEM (n = 4). *p < 0.05 compared with the values of vehicle groups. (C)
537 Representative immunofluorescent staining of lungs for DAPI (blue), neutrophil elastase (NE; green), and
538 citH3 (red) with phase contrast are shown (day 2).
539
540 Figure 2. BLM-induced NETs depended on the activity of peptidylarginine deiminases (PADs) both *in vivo*
541 and *in vitro*.
542 (A-D) WT mice received BLM (closed bar) or vehicle (open bar) intratracheally, following intraperitoneal
543 administration of Cl-amidine or vehicle once a day from the preceding the instillations of BLM or vehicle.
544 NETs were analyzed in the BAL fluid (BALF) and lung specimens on day 2. (A) Representative
545 immunofluorescent staining of BAL cells for DAPI (blue), NE (green), and citH3 (red). (B) The percentage of
546 NETs in BAL neutrophils of mice (n = 4). (C) The number of total cells and the percentage of macrophages,
547 neutrophils and lymphocytes in BAL cells (n = 4). (D) Representative immunofluorescent staining of lungs
548 for DAPI (blue), NE (green), and citH3 (red) with phase contrast. (E, F) Blood neutrophils were stimulated *in*
549 *vitro* by ionomycin (inducer of NETs), and BLM in the absence or presence of Cl-amidine, vehicle, DNAse-1
550 for 2.5 h. (E) Representative immunofluorescent staining for DAPI (blue), NE (green), and citH3 (red). (F)
551 The percentage of NETs in neutrophils (n = 4). Results for each group are expressed as means ± SEM. *p <
552 0.05, **p < 0.01 compared with the values of each group.
553
554 Figure 3. Deficiency of peptidylarginine deiminase 4 (PAD4) suppresses BLM-induced NETs and
555 inflammation associated gene expression.
556 WT and *Padi4* gene knockout (PAD4-KO) mice received BLM (closed bar) or vehicle (open bar)
557 intratracheally. BALF and lung specimens were analyzed on day 2. (A) The numbers of total cells and the
558 percentage of macrophages, neutrophils and lymphocytes in BAL cells of WT and PAD4-KO mice (n = 3-5).
559 (B) Representative immunofluorescent staining of BAL cells for DAPI (blue), NE (green), and citH3 (red).
560 (C) The percentage of NETs in BAL neutrophils (n = 3-5). (D) Representative immunofluorescent staining of
561 lungs for DAPI (blue), NE (green), and citH3 (red) with phase contrast. (E) The mRNA expression levels of
562 interleukin-6, tumor necrosis factor alpha, and interferon gamma were analyzed by quantitative real-time
563 polymerase chain reaction (qRT-PCR) (n = 5). Results for each group are expressed as means ± SEM. *p <
564 0.05, **p < 0.01 compared with the values of each group.
565
566 Figure 4. Deficiency of PAD4 suppresses BLM-induced pulmonary fibrosis and expression of fibrosis-related
567 genes.
568 WT and PAD4-KO mice received BLM or vehicle intratracheally. (A) Time course of changes in the body
569 weight of mice until day 21 (n = 8-17). (B) Survival rates of WT and PAD4-KO mice after BLM or vehicle
570 instillations (n = 8-17). (C) Masson's trichrome staining of lung tissue sections on day 21. (D) Fibrosis scores
571 and (E) collagen loads of WT and PAD4-KO mice received BLM (closed bar) or vehicle (open bar) on day 21
572 (n = 5). (F) The mRNA expression levels of collagen type I alpha 1 chain, elastin, fibronectin 1, smooth muscle
573 alpha actin, connective tissue growth factor, fibroblast growth factor 2 and transforming growth factor beta 1
574 were analyzed by qRT-PCR (n = 5). Results for each group are expressed as means ± SEM. *p < 0.05, **p <

575 0.01 compared with the values of each group.
576
577 Figure 5. Deficiency of PAD4 contributes to the changes in the number of alveolar epithelial cells, pulmonary
578 vascular endothelial cells (PVECs), and α-smooth muscle actin (SMA) positive mesenchymal cells.
579 WT and PAD4-KO mice received BLM (closed bar) or vehicle (open bar) intratracheally. On day 14, the
580 number of (A) total lung cells, (B) type-I ($AQP5^{+}/CD31^{-}/CD45^{-}$), and (C) type-II ($SP\text{-}C^{+}/CD31^{-}/CD45^{-}$)
581 alveolar epithelial cells, (D) PVECs ($CD31^{+}/CD45^{-}$), as well as (E) α-SMA positive mesenchymal cells (α-
582 $SMA^{+}/CD31^{-}/CD45^{-}$) of WT and PAD4-KO mice on day 14 after BLM or vehicle instillations were analyzed
583 by flow cytometry (n = 3-5). Results for each group are expressed as means ± SEM. *$p < 0.05$ compared with
584 the values of each group.
585
586 Figure 6. Bone marrow (BM) derived cells from PAD4-KO mice ameliorate BLM-induced pulmonary fibrosis
587 in WT mice.
588 (A) Assessment of the reconstitution of chimeric animals. GFP mice were irradiated and grafted with BM cells
589 from PAD4-KO mice. The percentage of GFP negative cells in the population of peripheral blood cells of GFP
590 mice at each time point are shown (n = 3). (B-D) WT mice were irradiated and grafted with BM cells from
591 WT (open bar) or PAD4-KO (closed bar) mice. Chimeric mice received BLM 6 wk after BM transplantation.
592 (B) The flow scheme of the experiment. (C) 21 days after BLM instillations, lung sections of WT chimeric
593 mice were stained with Masson's trichrome staining. (D) Fibrosis scores of both groups on day 21 after BLM
594 instillations were calculated (n = 5). Results for each group are expressed as means ± SEM. *$p < 0.05$ compared
595 with the values of each group.
596
597

Figure 1A

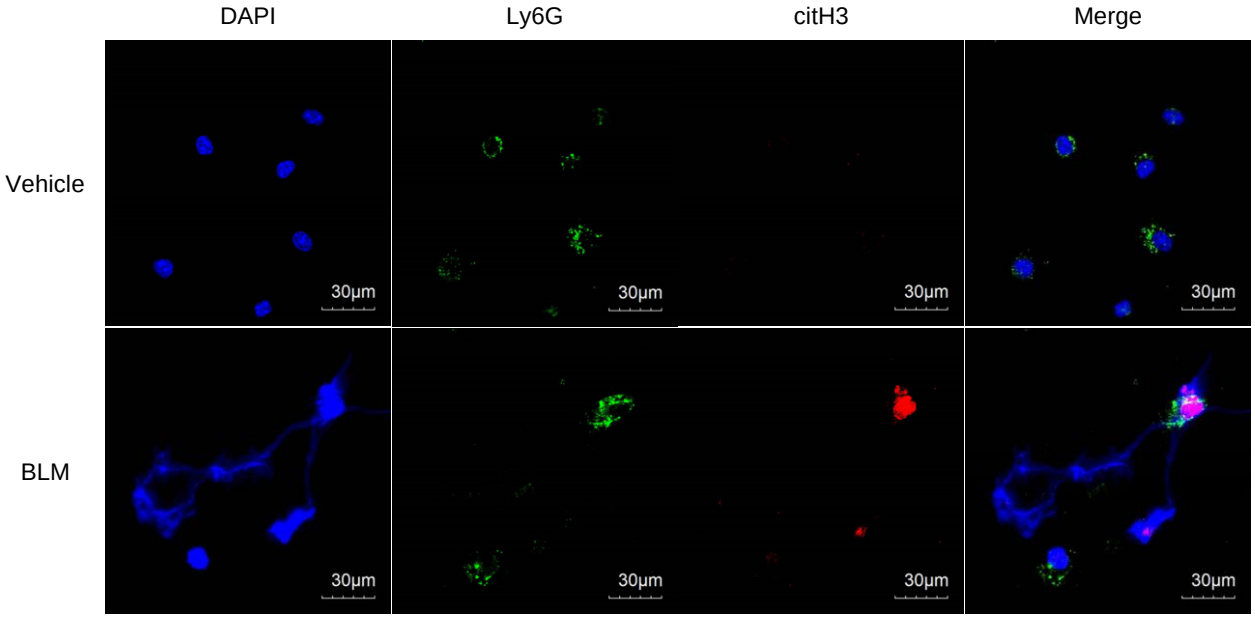

Figure 1B

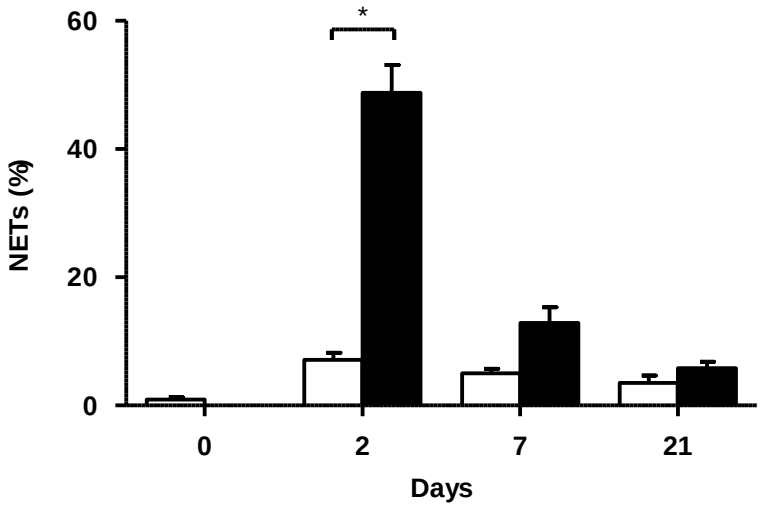

Figure 1C

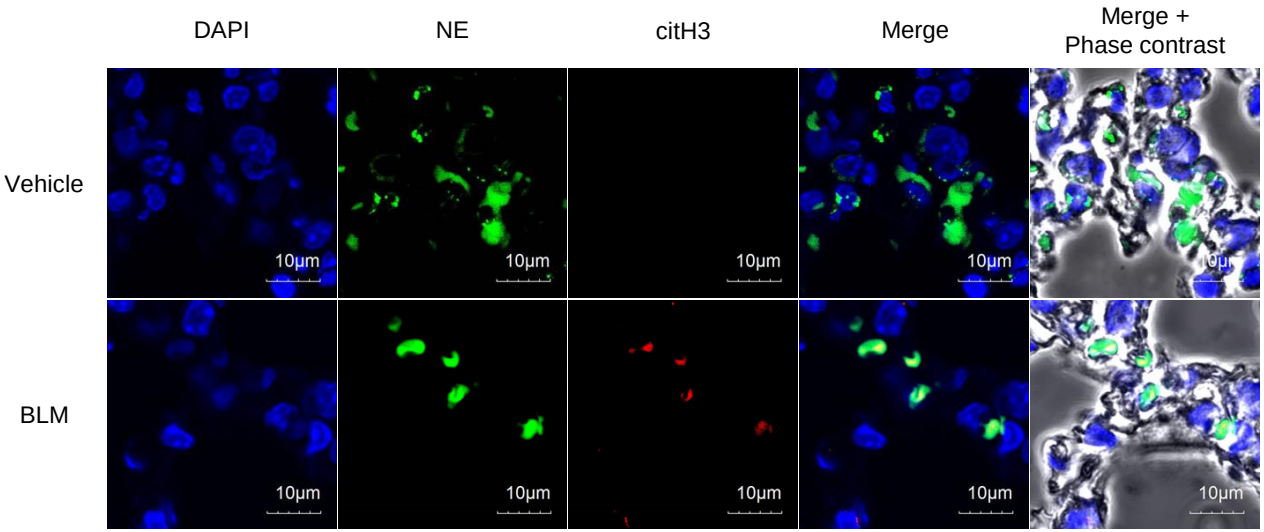

Figure 2A

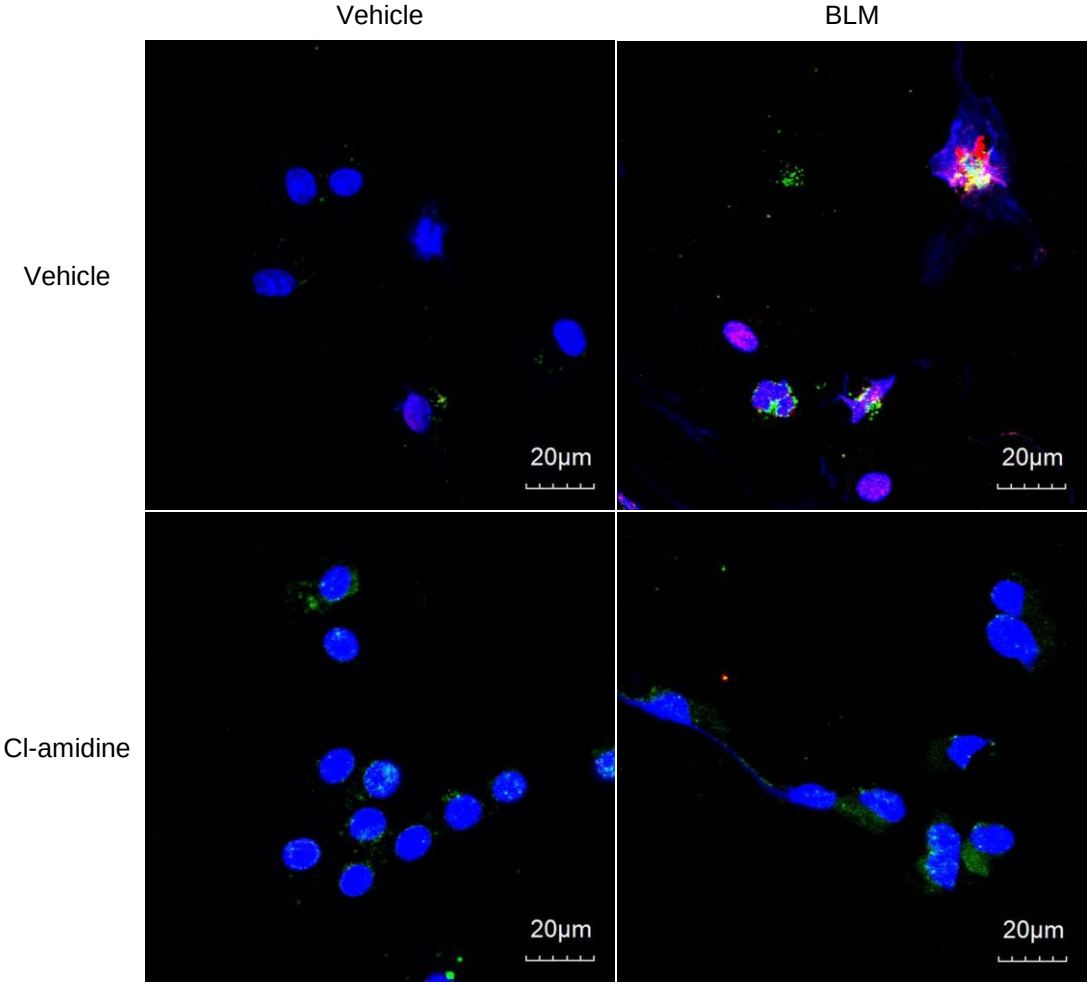

Figure 2B

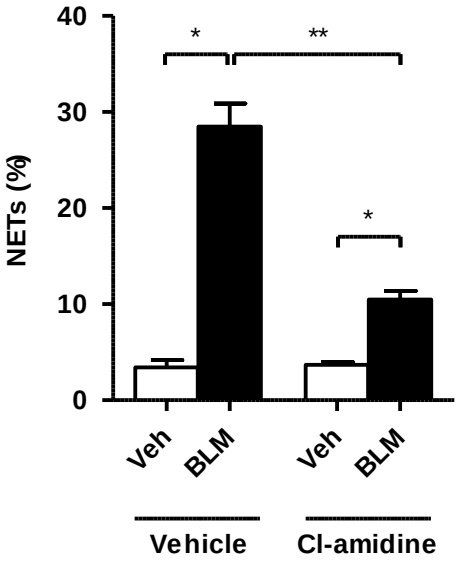

Figure 2C

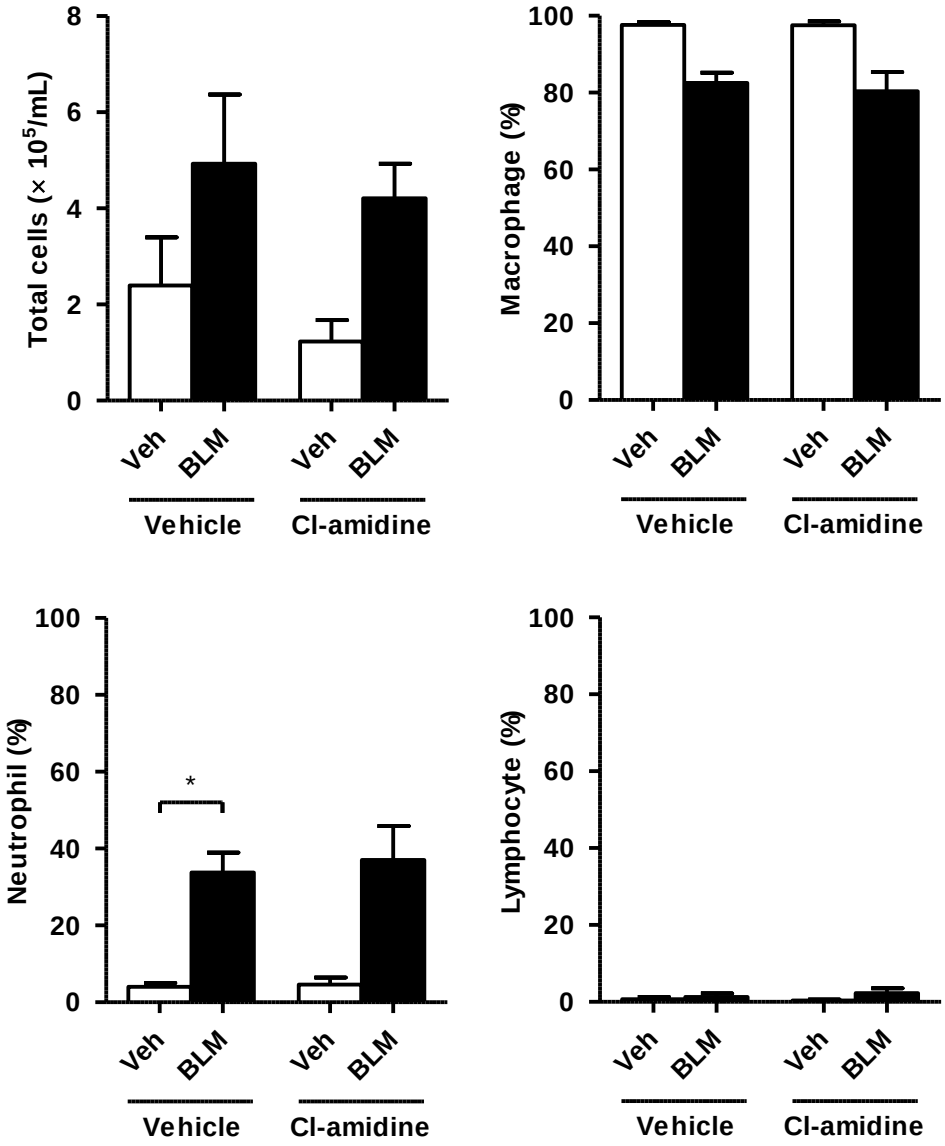
Total cells (× 10^5/mL)
8
6
4
2
0
Veh
BLM
Veh
BLM
Vehicle
Cl-amidine
Macrophage (%)
100
80
60
40
20
0
Veh
BLM
Veh
BLM
Vehicle
Cl-amidine
Neutrophil (%)
100
80
60
40
20
0
*
Veh
BLM
Veh
BLM
Vehicle
Cl-amidine
Lymphocyte (%)
100
80
60
40
20
0
Veh
BLM
Veh
BLM
Vehicle
Cl-amidine

Figure 2D

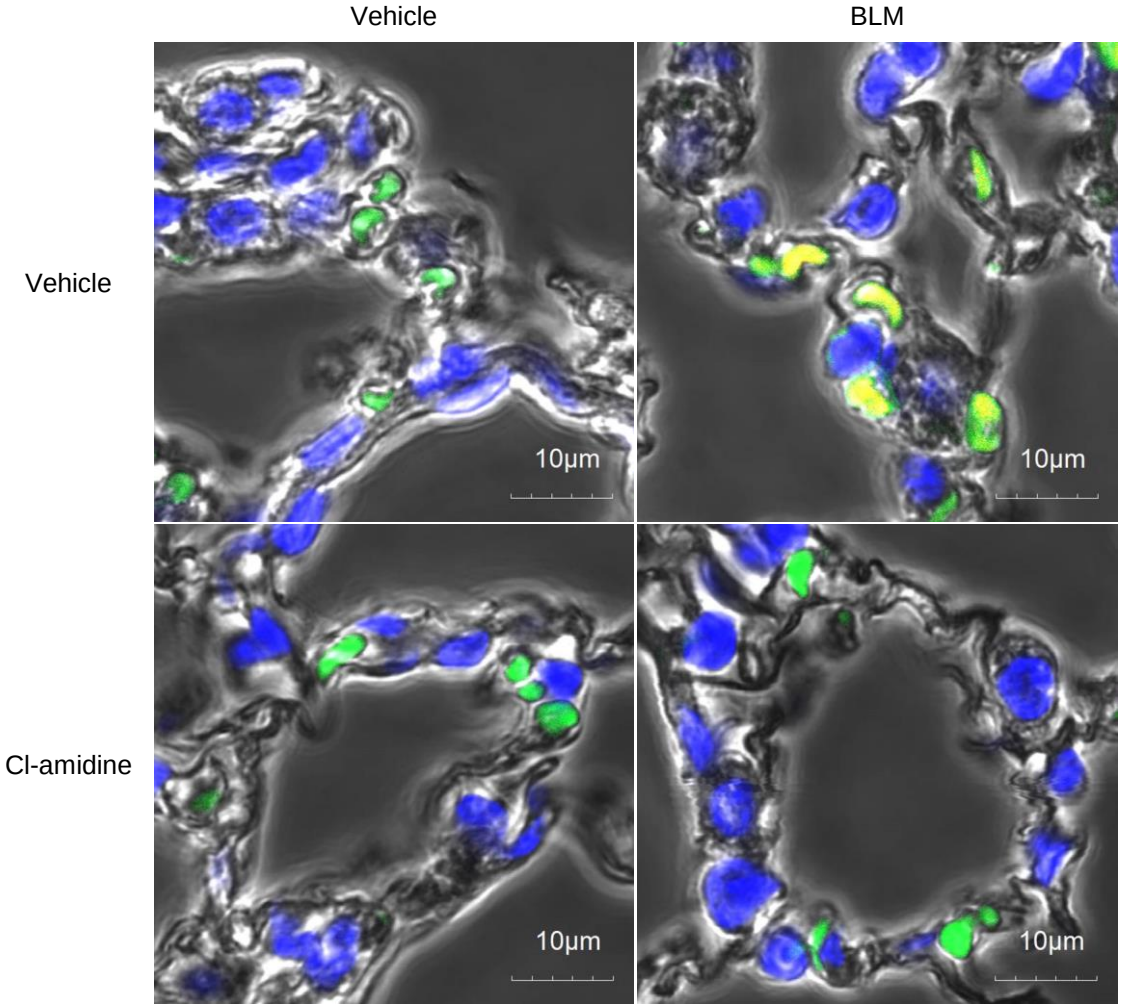

Figure 2E

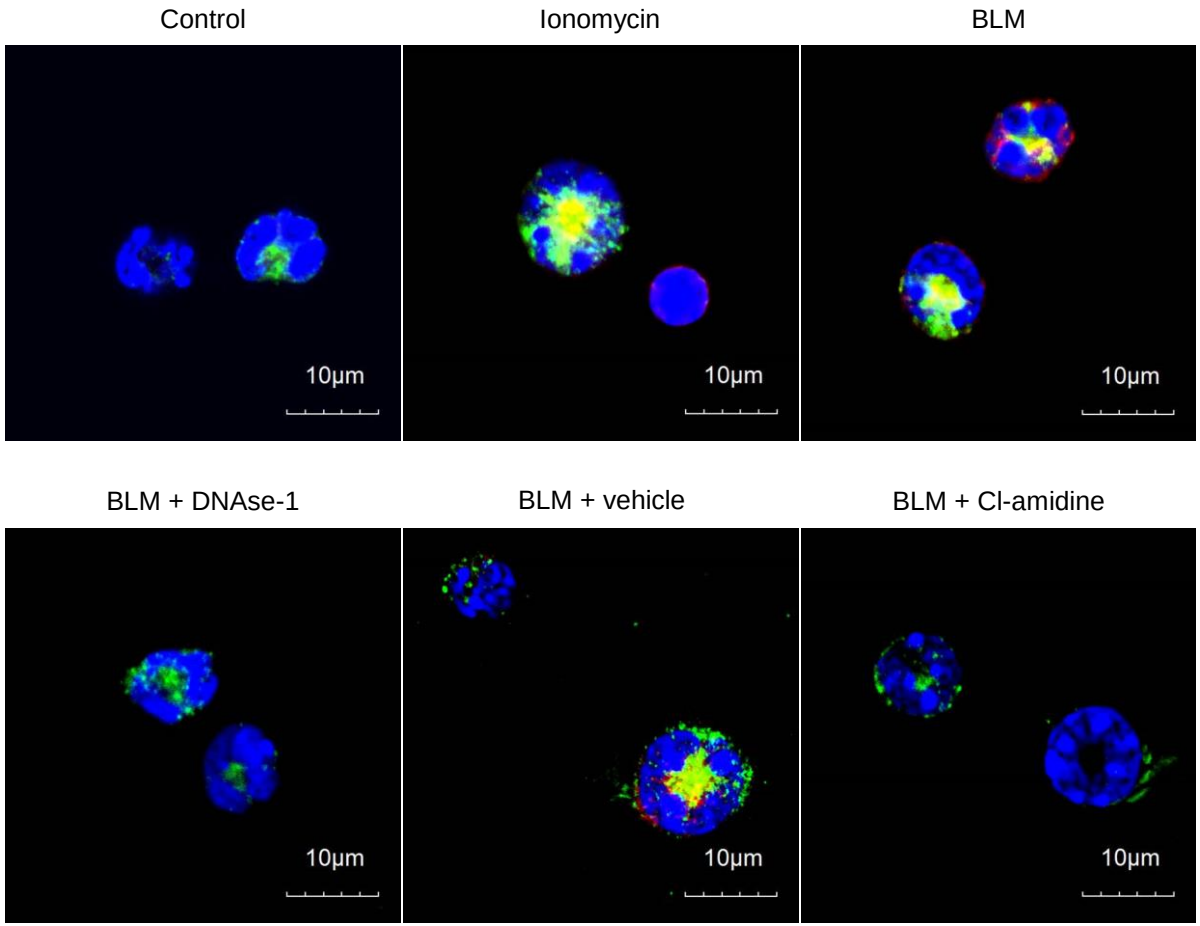
Control
Ionomycin
BLM
BLM + DNAse-1
BLM + vehicle
BLM + Cl-amidine
10μm
10μm
10μm
10μm
10μm
10μm

Figure 2F

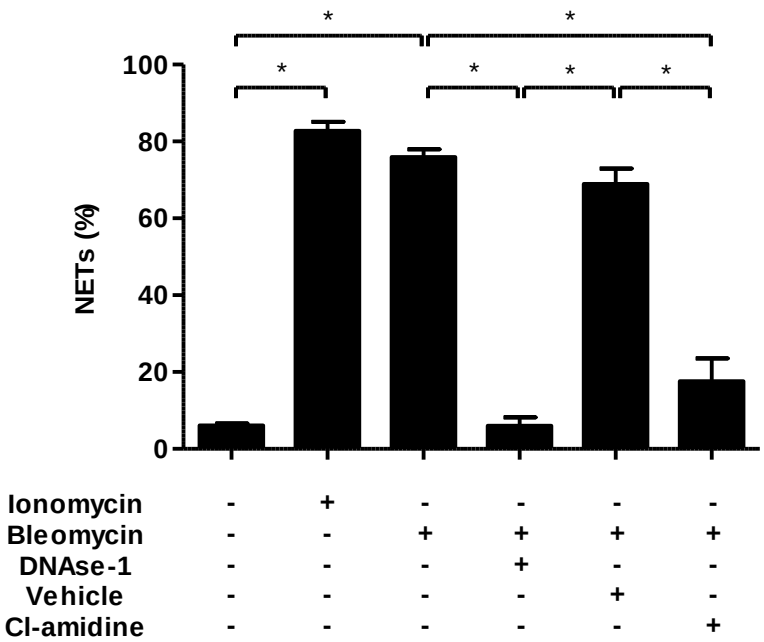
*
*
*
*
*
*
100
80
60
40
20
0
NETs (%)
Ionomycin - + - - - -
Bleomycin - - + + + +
DNAse-1 - - - + - -
Vehicle - - - - + -
Cl-amidine - - - - - +

Figure 3A

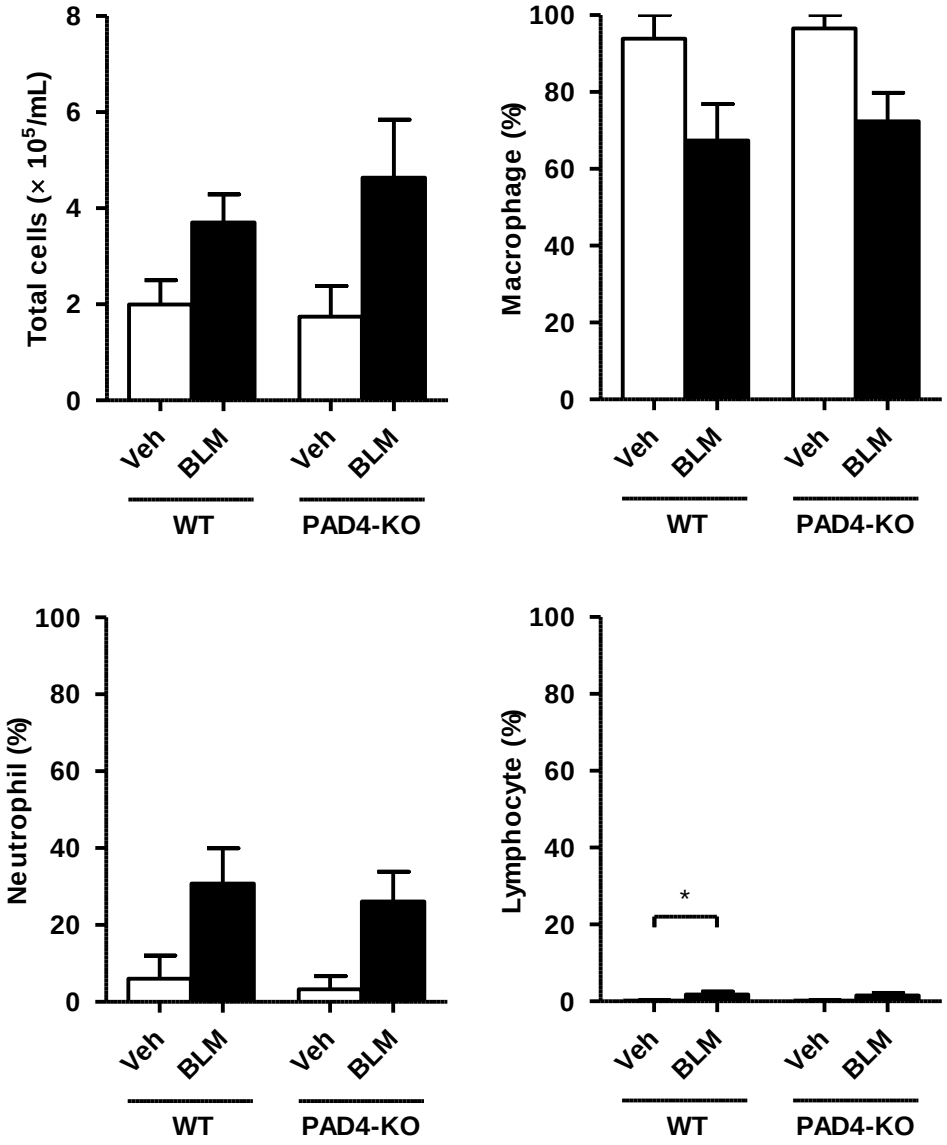
Total cells (× 10^5/mL)
8
6
4
2
0
Veh
BLM
Veh
BLM
WT
PAD4-KO
Macrophage (%)
100
80
60
40
20
0
Veh
BLM
Veh
BLM
WT
PAD4-KO
Neutrophil (%)
100
80
60
40
20
0
Veh
BLM
Veh
BLM
WT
PAD4-KO
Lymphocyte (%)
100
80
60
40
20
0
*
Veh
BLM
Veh
BLM
WT
PAD4-KO

Figure 3B

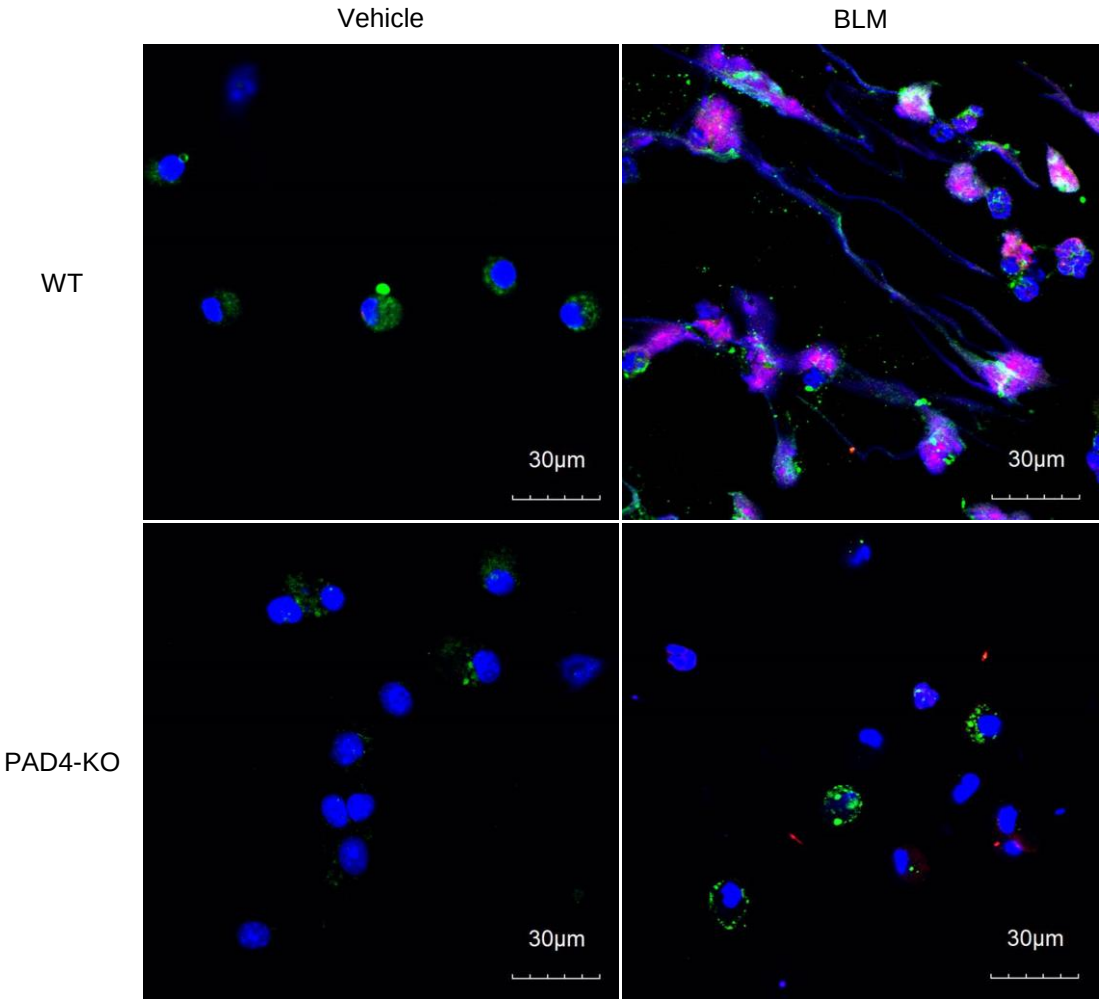

Figure 3C

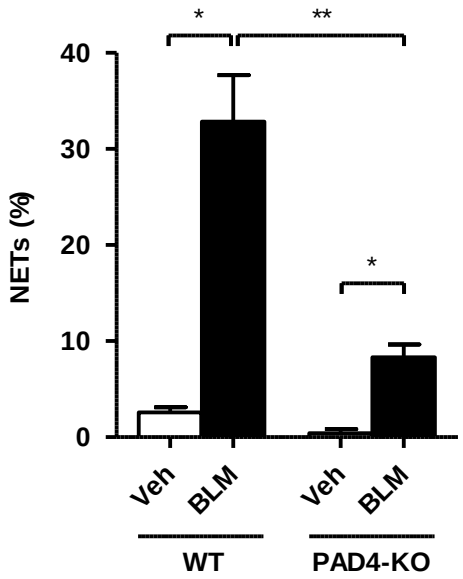

Figure 3D

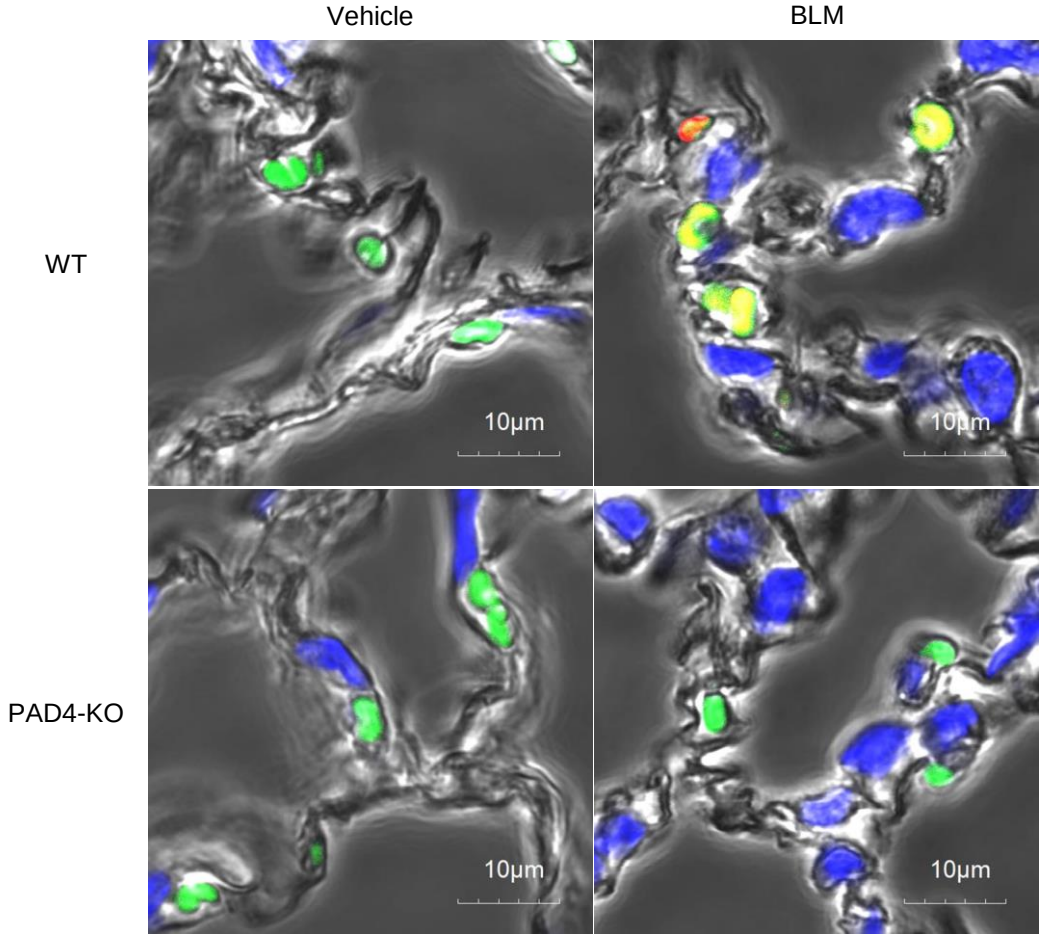

Figure 3E

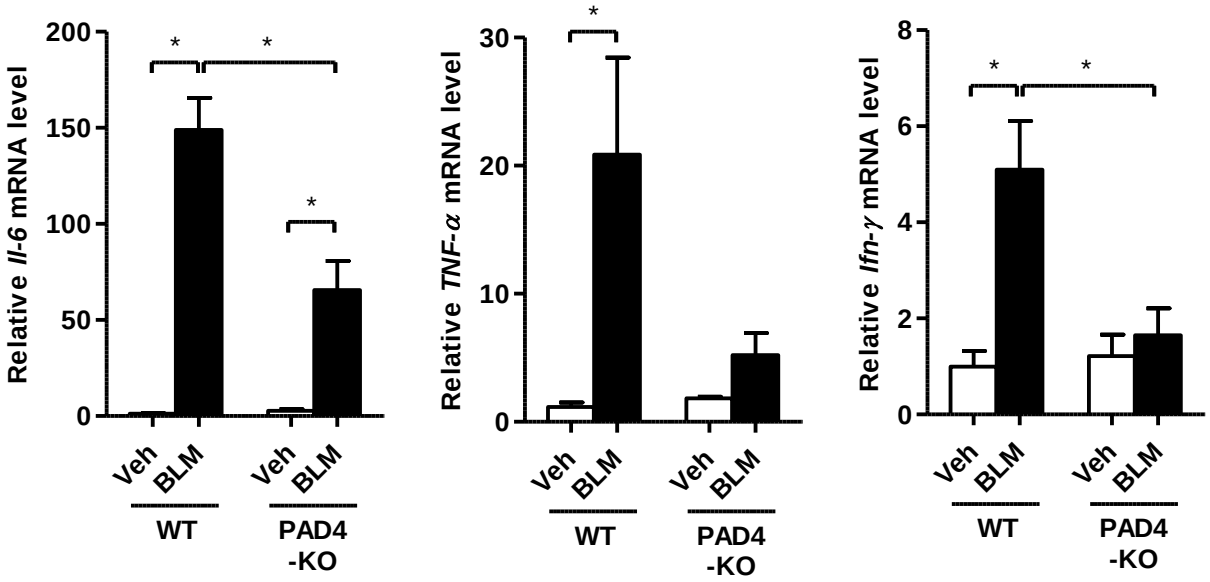
Relative Il-6 mRNA level
200
150
100
50
0
*
*
*
Veh
BLM
Veh
BLM
WT
PAD4
-KO
Relative TNF-α mRNA level
30
20
10
0
*
Veh
BLM
Veh
BLM
WT
PAD4
-KO
Relative Ifn-γ mRNA level
8
6
4
2
0
*
*
Veh
BLM
Veh
BLM
WT
PAD4
-KO

Figure 4A

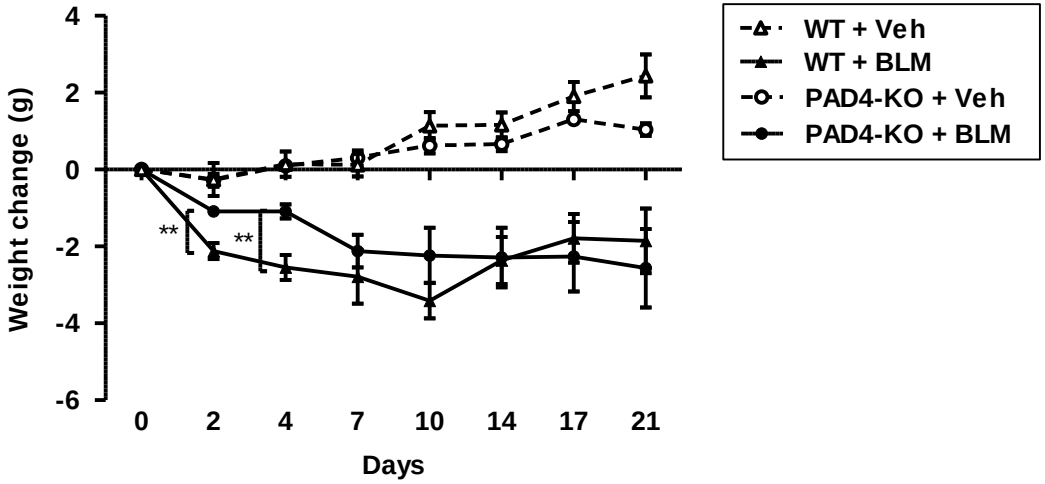
4
2
0
-2
-4
-6
Weight change (g)
**
**
0
2
4
7
10
14
17
21
Days
WT + Veh
WT + BLM
PAD4-KO + Veh
PAD4-KO + BLM

Figure 4B

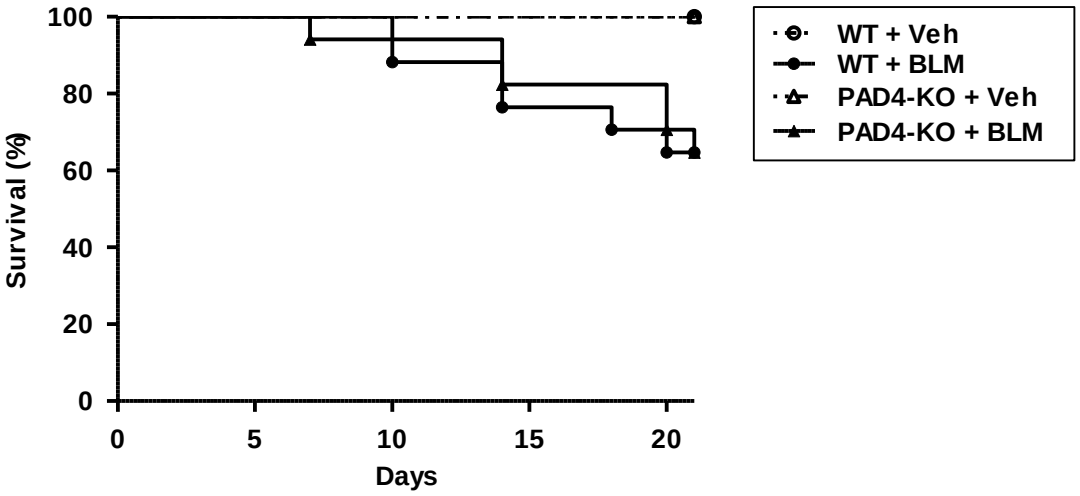
100
80
60
40
20
0
Survival (%)
0
5
10
15
20
Days
WT + Veh
WT + BLM
PAD4-KO + Veh
PAD4-KO + BLM

Figure 4C

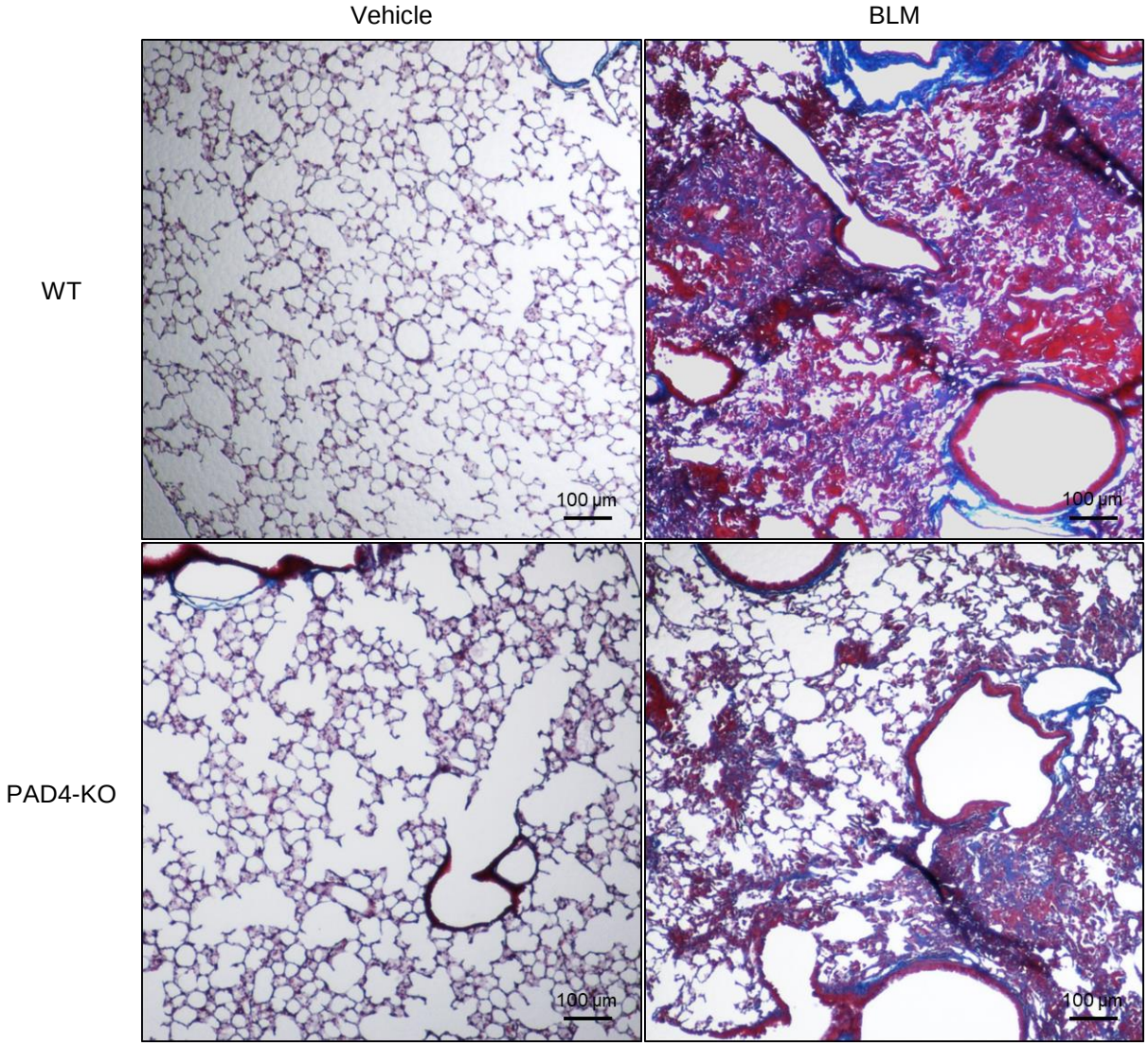

Figure 4D

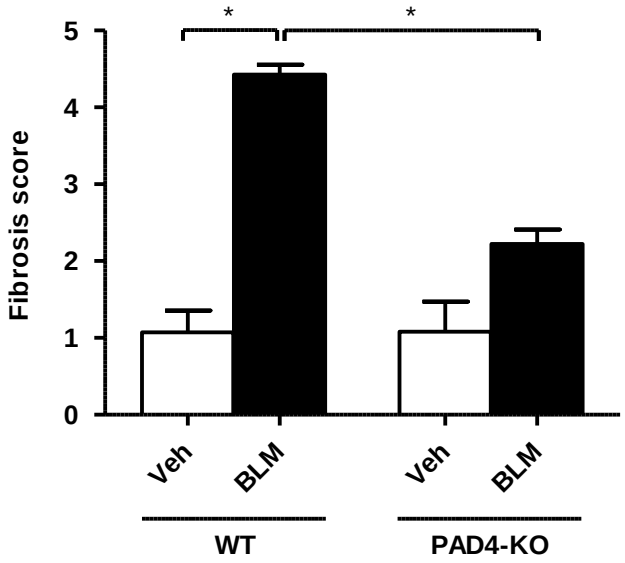

Figure 4E

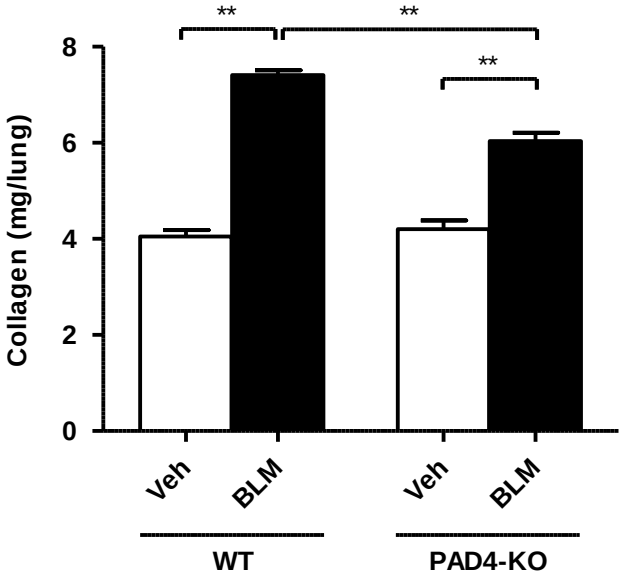

Figure 4F

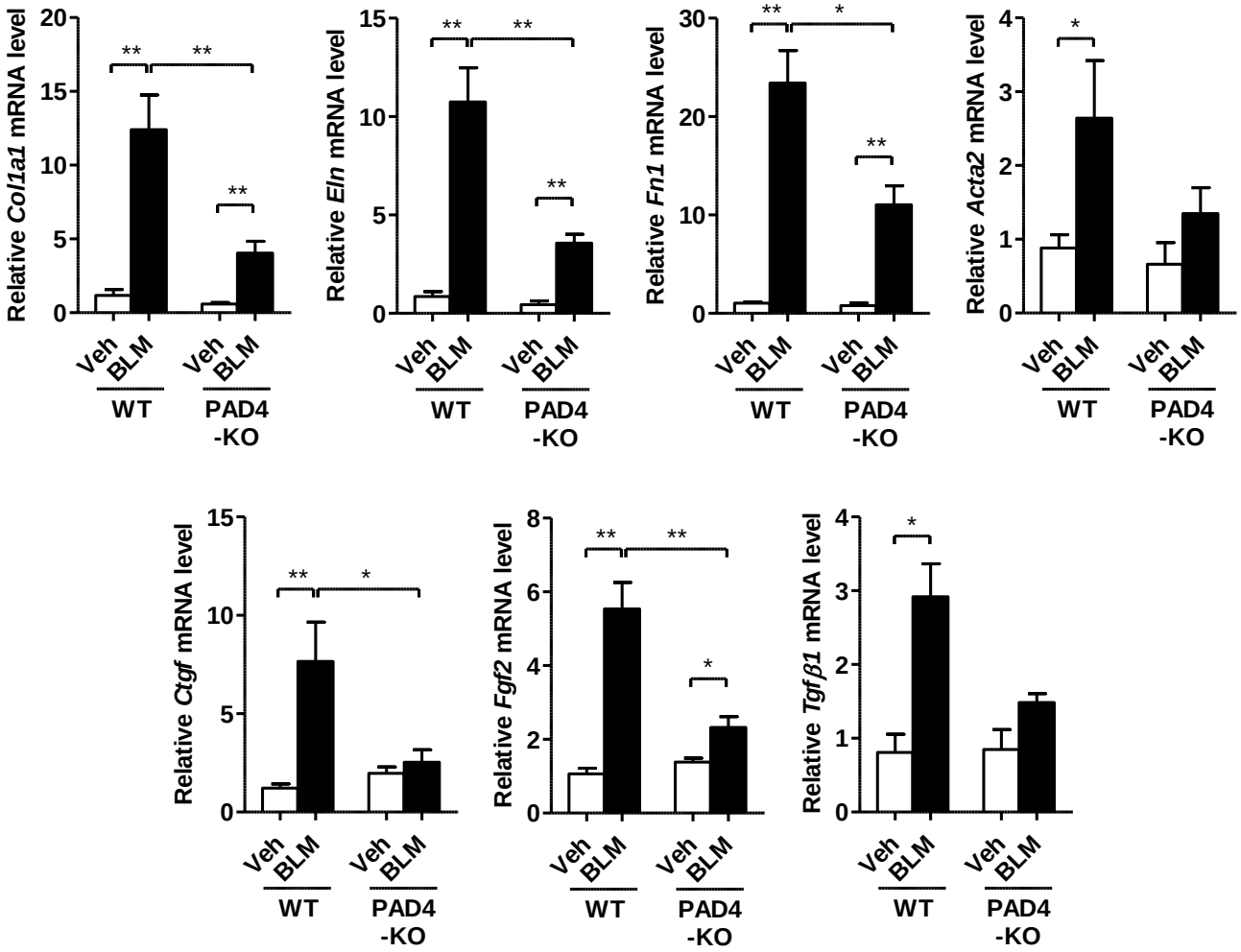
Relative Col1a1 mRNA level
Relative Eln mRNA level
Relative Fn1 mRNA level
Relative Acta2 mRNA level
Relative Ctgf mRNA level
Relative Fgf2 mRNA level
Relative Tgfβ1 mRNA level
Veh
BLM
WT
PAD4
-KO
**
*

Figure 5A

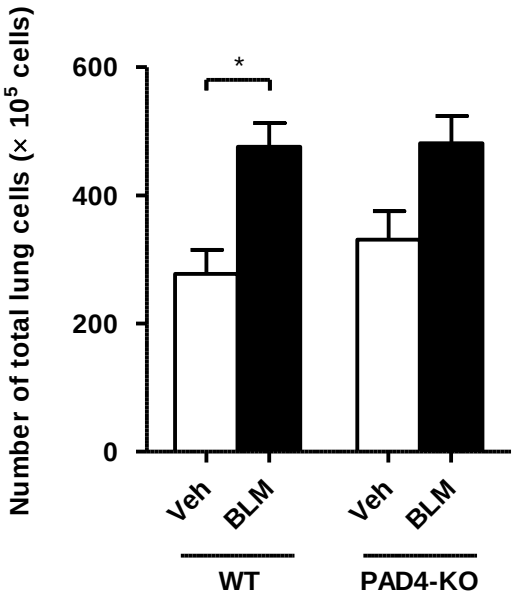
Number of total lung cells (× 10^5 cells)
600
400
200
0
*
Veh
BLM
Veh
BLM
WT
PAD4-KO

Figure 5B

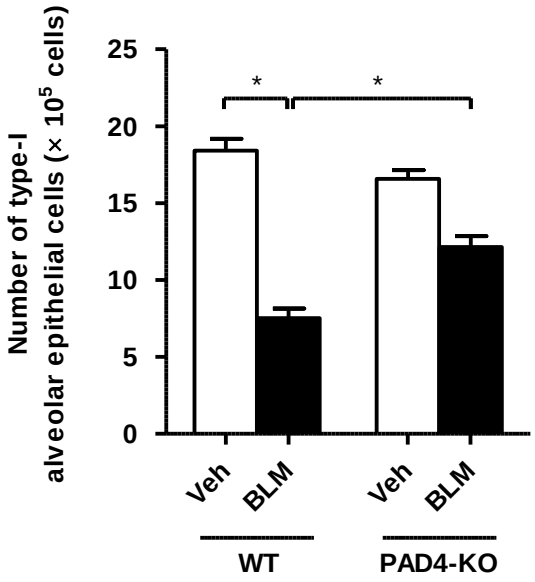
Number of type-I
alveolar epithelial cells (× 10^5 cells)
25
20
15
10
5
0
*
*
Veh
BLM
Veh
BLM
WT
PAD4-KO

Figure 5C

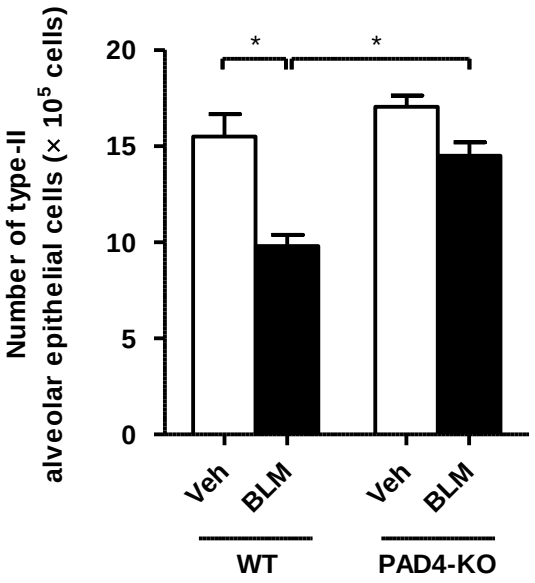
Number of type-II
alveolar epithelial cells (× 10^5 cells)
20
15
10
5
0
*
*
Veh
BLM
Veh
BLM
WT
PAD4-KO

Figure 5D

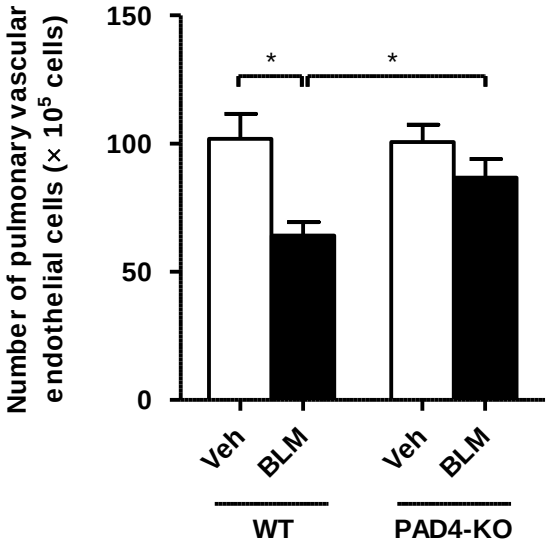
Number of pulmonary vascular endothelial cells (× 10^5 cells)
150
100
50
0
*
*
Veh
BLM
Veh
BLM
WT
PAD4-KO

Figure 5E

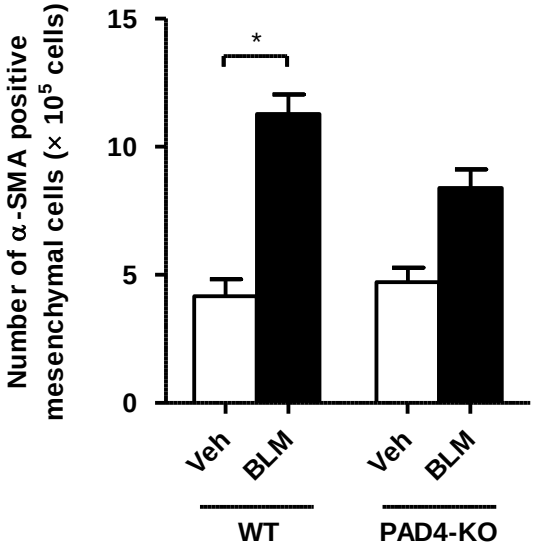
Number of α-SMA positive mesenchymal cells (× 10^5 cells)
15
10
5
0
*
Veh
BLM
Veh
BLM
WT
PAD4-KO

Figure 6A

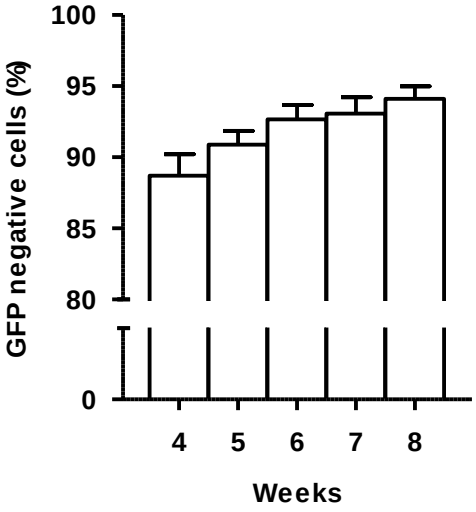

Figure 6B

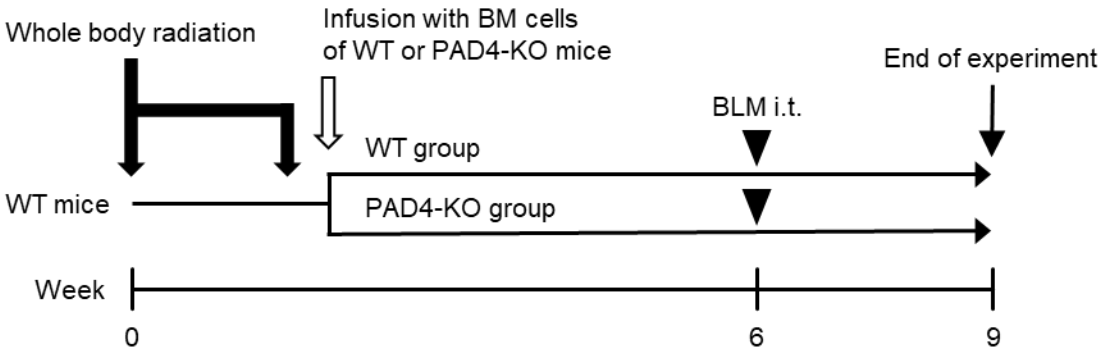
Whole body radiation
Infusion with BM cells
of WT or PAD4-KO mice
End of experiment
BLM i.t.
WT group
WT mice
PAD4-KO group
Week
0
6
9

Figure 6C

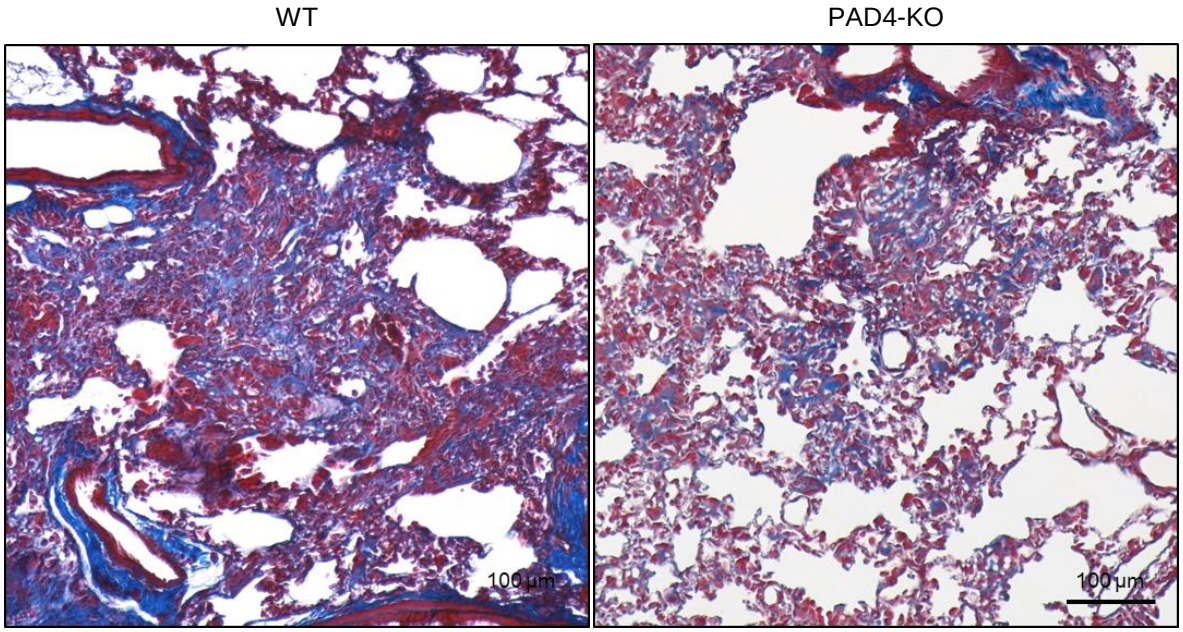

Figure 6D

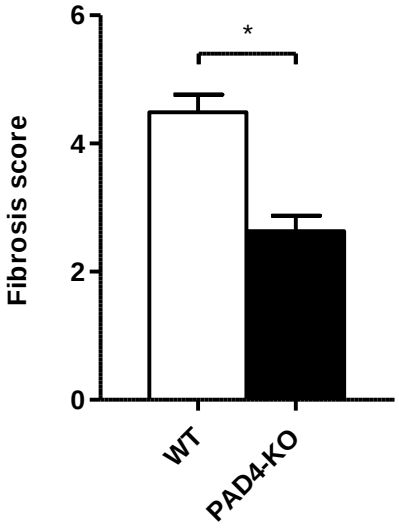

Supplementary Materials and Methods

Murine model of pulmonary fibrosis

Mice were anesthetized using a cocktail of medetomidine, midazolam and butorphanol and intratracheally administered with 3 U/kg of bleomycin (BLM; Nippon Kayaku, Tokyo, Japan) dissolved in 100 µL saline (Otsuka Pharmaceutical Factory, Tokyo, Japan) or vehicle. Cl-amidine (Cayman Chemical, Ann Arbor, MI, USA) was reconstituted in ethanol to make a stock solution of 20 mg/mL. Stocked Cl-amidine was diluted with PBS to a concentration of 2.0 mg/mL and was intraperitoneally injected on the same, previous and following day of administration of BLM or vehicle.

Histological examination

Lungs were inflated by 4 % (wt/vol) paraformaldehyde (PFA) with a pressure of 20 cm H_2O. Keeping lung inflated, lungs were resected and fixed in 4% PFA for 24 h. Then, they were embedded in paraffin. Lung sections (2 µm) were deparaffinized in xylene, hydrated using methanol, and stained with Masson's trichrome. Histological images were scanned and captured using a Nikon Eclipse 55i; microscope (Nikon Corporation, Tokyo, Japan). The extent of lung fibrosis was assessed using the Ashcroft scale in a blinded test.

Detection of neutrophil extracellular traps (NETs) in lungs

Deparaffinized and dehydrated lung sections (2 µm) were incubated in citrate buffer (pH 6.0) (Abcam, Cambridge, UK) for 10 min at 50 °C. After cooling below 30 °C, lungs sections were permeabilized with 0.5 % Triton-X (Sigma, St. Louis, MO, USA) for 5 min, blocked with 0.05 % Tween 20 (Chem Cruz Biochemicals, Santa Cruz, CA, USA) and 2 % normal goat serum blocking solution (Vector Laboratories, Inc., Burlingame, CA, USA) for 30 min, and incubated with primary antibodies at 4 °C overnight. After incubation with secondary antibodies, lung sections were mounted with DAPI (4′-6-diamidino-2-phenylindole dihydrochloride) (Vector Laboratories, Inc.), and observed under a confocal microscope (Fluoview FV 10i; Olympus, Tokyo, Japan).

Quantitative polymerase chain reaction (qPCR) analysis

Total RNA was isolated from resected right upper lung using RNeasy Fibrous Tissue Mini Kit (Qiagen, Hilden, Germany). RNA was subjected to reverse-transcription PCR with the RT^2 First Strand Kit (Qiagen). cDNA samples were subjected to qPCR using the Fast SYBR Green Master Mix (Thermo Fisher Scientific, Waltham, MA, USA) in an ABI 7300 Real-Time PCR System (Applied Biosystems, Foster City, CA, USA). Specific primers were designed using the web software of Universal Probe Library Assay Design Center (https://lifescience.roche.com/global_en.html). The expression level of each target gene was normalized against threshold cycle (Ct) values of Rn18s and calculated using the $2^{-\Delta\Delta}$ Ct method.

The following primers were used: IL-6 forward, 5′-GCT ACC AAA CTG GAT ATA ATC AGG A-3′ and IL-6 reverse, 5′-CCA GGT AGC TAT GGT ACT CCA GAA-3′. Tnfα forward, 5′-GGT CTG GGC CAT AGA ACT GA-3′ and Tnfα reverse, 5′-TCT TCT CAT TCC TGC TTG TGG-3′. Ifnγ forward, 5′-ATC TGG AGG AAC TGG CAA AA-3′ and Ifnγ reverse, 5′-TTC AAG ACT TCA AAG AGT CTG AGG TA-3′. Col1a1 forward, 5′-CCG CTG GTC AAG ATG GTC-3′ and Col1a1 reverse, 5′-CTC CAG CCT TTC CAG GTT CT-3′. Eln forward, 5′-TGG AGC AGG ACT TGG AGG T-3′ and Eln reverse, 5′-CCT CCA GCA CCA TAC TTA GCA-3′. Fn1 forward, 5′-CGA TAT TGG TGA ATC GCA GA-3′ and Fn1 reverse, 5′-CGG AGA GAG TGC CCC TAC TA-3′. Acta2 forward, 5′-CTC TCT TCC AGC CAT CTT TCA T-3′ and Acta2 reverse, 5′-TAT AGG TGG TTT CGT GGA TGC-3′. Ctgf forward, 5′-TGA CCT GGA GGA AAA CAT TAA GA-3′ and Ctgf reverse, 5′-AGC CCT GTA TGT CTT CAC ACT G-3′. Fgf2 forward, 5′-CGG CTC TAC TGC AAG AAC G-3′ and Fgf2 reverse, 5′-TGC TTG GAG TTG TAG TTT GAC G-3′. Tgfβ1 forward, 5′-CAG CAG CCG GTT ACC AAG-

3′ and Tgfβ1 reverse, 5′-TGG AGC AAC ATG TGG AAC TC-3′. Rn18s forward, 5′-GCA ATT ATT CCC CAT GAA CG-3′ and Rn18s reverse, 5′-GGG ACT TAA TCA ACG CAA GC-3′. Rn18s was used as the housekeeping gene for data normalization.

Flow cytometric assay

After intratracheal instillations of BLM or vehicle, mouse lungs were resected on day 14, minced to less than 1-mm fragments, and digested with Collagenase (Wako, Tokyo, Japan), Dispase II (Sigma) and DNAse-1 (Wako) for 1 h at 37 °C. After washing, the number of cells was counted, and cells were seeded onto 96-well round-bottom plates. Cells were stained with FITC-CD45, Alexa Fluor 700-CD45, PE/Cy7-CD31, anti-Aquaporin 5, SP-C, and α-actin smooth muscle antibodies. After staining with secondary antibodies, multicolor analysis was conducted on FACS Canto II (Becton Dickinson, Franklin Lakes, NJ, USA).

Sircol collagen assay

Whole mouse lungs were resected and immediately frozen at -80 °C. Thawed lungs were dried at 30 °C for 24 h. Lungs were homogenized and incubated in 0.5 M acetic acid with 0.1 mg/mL pepsin solution for 24 h. Extracted lysate was measured using the Sircol Collagen Assay Kit (Biocolor Ltd., Carrickfergus, UK) according to manufacturer's instruction.

Bone marrow (BM) reconstitution and BLM inducing pulmonary fibrosis

Recipient wild-type (WT) mice (C57BL/6, 8 wk old) were irradiated with 5 and 4.5 Gy, 5 h apart. Donor mice BM cells were obtained by flushing bilateral femur and tibia of WT and *Padi4* gene knockout (PAD4-KO) mice. After second radiation, donor BM cells (3×10^7 cells) were immediately injected via the tail vein. After 6 wk, BLM was administered intratracheally. After 3 wk , mice were sacrificed.

C57BL/6 mice expressing enhanced green fluorescent protein (GFP) under the control of a CAG promoter (GFP-Tg mice, Japan SLC, Shizuoka, Japan) were used as recipient, whereas PAD4-KO mice were used as donor. The percentages of GFP negative cells in the population of peripheral blood cells was evaluated by flow cytometry.

Reagent

For immunofluorescent staining with bronchoalveolar lavage cells, rat Alexa Fluor 488-conjugated anti-mouse Ly6G monoclonal antibody (1:100; BioLegend, San Diego, CA, USA, 127626), sheep anti-human neutrophil elastase polyclonal antibody (1:200; LSBio, Seattle, WA, USA, LS-B4244), and rabbit anti-histone H3 (citrulline R2 + R8 + R17) polyclonal antibody (1:250; Abcam, 5103) were used as primary antibodies. Alexa Fluor 488 donkey anti-sheep IgG polyclonal antibody (1:250; Invitrogen, Carlsbad, CA, USA, A-11015) and Alexa Fluor 594 donkey anti-rabbit IgG polyclonal antibody (1:500; Invitrogen, A-21207) were used as secondary antibodies.

For immunohistochemistry with paraffinized sections, sheep anti-human neutrophil elastase polyclonal antibody (1:200; LSBio) and rabbit anti-histone H3 (citrulline R2 + R8 + R17) polyclonal antibody (1:100; Abcam, 5103) were used as primary antibodies. Alexa Fluor 488 donkey anti-sheep IgG polyclonal antibody (1:1000; Invitrogen, A-11015) and Alexa Fluor 594 donkey anti-rabbit IgG polyclonal antibody (1:1000; Invitrogen, A-21207) were used as secondary antibodies. All primary and secondary antibodies were diluted in PBS.

For flow cytometric analysis, PE/Cy7 rat anti-mouse CD31 monoclonal antibody (BioLegend, 102418), FITC rat anti-mouse CD45 monoclonal antibody (BioLegend, 103108), Alexa Fluor700 rat anti-mouse CD45 monoclonal antibody (BioLegend, 103127), rabbit anti-Aquaporin 5 polyclonal antibody (Abcam, ab78486), goat anti-SP-C (M-20) polyclonal antibody (Santa Cruz Biotechnology, Santa Cruz, CA, USA, sc-7706), and

rabbit anti-actin smooth muscle polyclonal antibody (Thermo Fisher Scientific, RB-9010-P1) were used as primary antibodies. Donkey anti-rabbit IgG polyclonal antibody (Invitrogen, A-21206), donkey anti-goat IgG polyclonal antibody (Invitrogen, A-21084), and donkey anti-rabbit IgG polyclonal antibody (Invitrogen, 12-4739-81) were used as secondary antibodies.

Statistical analysis

All quantitative data are presented as means ± SD. Comparison among groups was performed by Mann-Whitney *U* test. Kaplan-Meier method was used for survival rate, and differences were analyzed by log-rank test. All p-values less than 0.05 was considered statistically significant. GraphPad Prism software (version 5.03; GraphPad Software, San Diego, CA, USA) was used for statistical analysis.

Supplementary Figure legend

Figure S1. Profiles of bronchoalveolar lavage (BAL) cells and fibrosis scores in wild-type (WT) mouse induced bleomycin (BLM) or vehicle.

WT mice received BLM (closed bar) or vehicle (open bar) intratracheally. BAL fluid and lung specimens were analyzed on day 2, 7 and 21. (A) The numbers of total cells and the percentage of macrophages, neutrophils and lymphocytes in BAL cells. (B) Fibrosis scores of WT mice received BLM (closed bar) or vehicle (open bar) on day 21. Results for each group are expressed as means ± SEM ($n = 5$). *$p < 0.05$, **$p < 0.01$, ***$p < 0.001$ compared with the values of each group.

Figure S1A

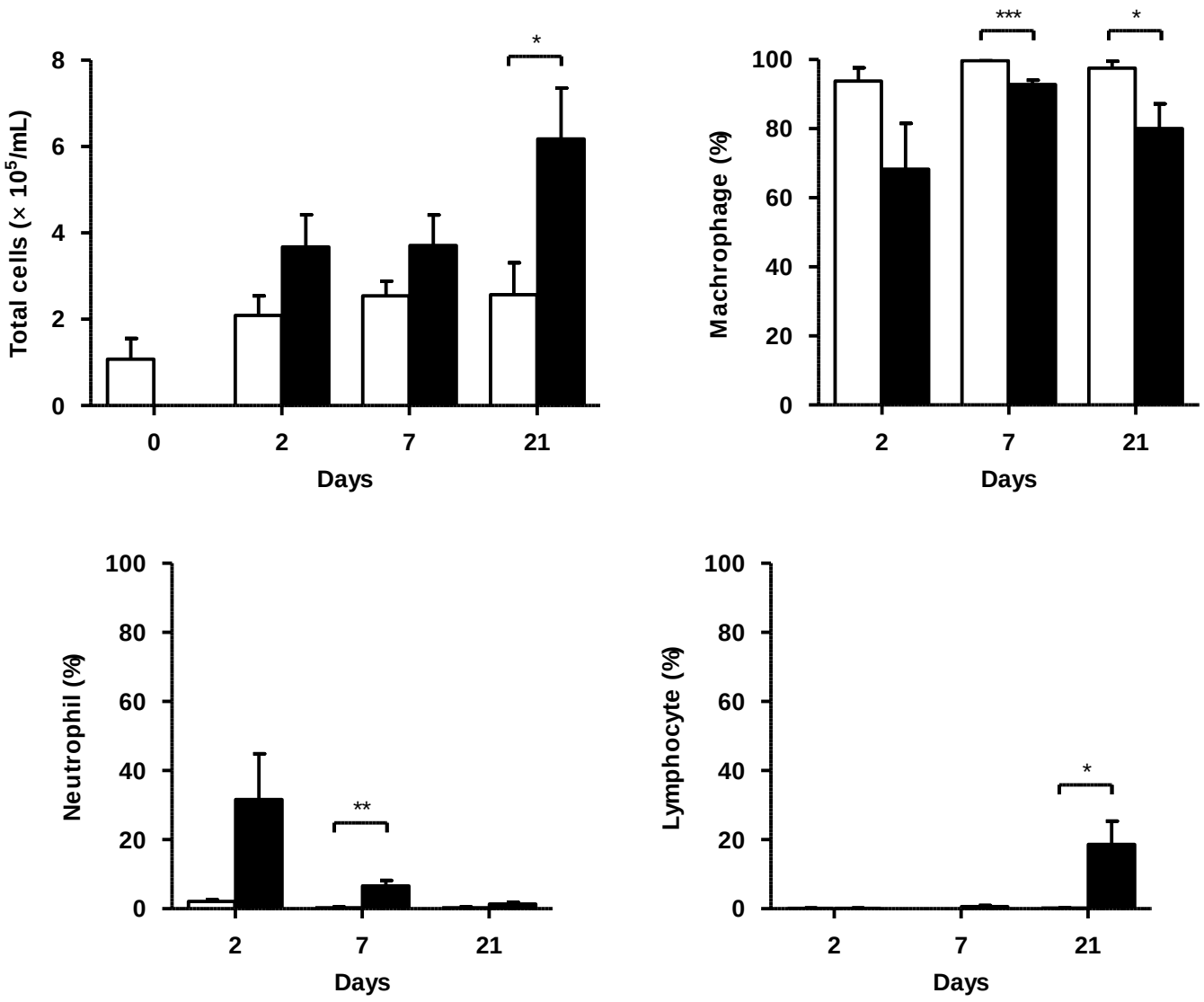
Total cells (× 10^5/mL)
8
6
4
2
0
*
0
2
7
21
Days
Machrophage (%)
100
80
60
40
20
0
***
*
2
7
21
Days
Neutrophil (%)
100
80
60
40
20
0
**
2
7
21
Days
Lymphocyte (%)
100
80
60
40
20
0
*
2
7
21
Days

Figure S1B